Hydrodynamics of ciliates at the air-liquid interface

Tohoku University

Department of biomedical engineering

Hydrodynamics of ciliates at the air-liquid interface

Jonathan Ferracci

March 21, 2013

Abstract

The importance of water-air interfaces on microorganism activities have been recognized by many researchers. Kristiansen et al. (1996) [1], for instance, highlighted the importance of water-air interfaces (WAI) in the growth rate of *Tetrahymena*. They clarified that the ratio of the surface-area to the depth of the culture vessel considerably affected the survival rate of *Tetrahymena*. On the other hand, in the case of bacteria, a biofilm may be formed at the water-air interface. Several groups have investigated the effects of surfactant on the interaction of bacteria with hydrophobic interfaces, such as water-gas interface. They have shown that the addition of surfactant prevents biofilm formation at any kind of interfaces, [2, 3]. These former studies clearly illustrated the biological importance of the water-air interface in the growth rate and formation of biofilm for microorganisms. However, in term of fluid mechanics, the behavior of swimming microorganism at the water-air interface have not been clarified to date. Although behaviors at the water-solid interface have been investigated extensively ([4, 5, 6, 7]), the one at liquid-air interface still remains unclear. In this thesis we report the new phenomenon of the entrapment of ciliated cells at the water-air interface, that is, the cells swim in two-dimension at the interface for more than tens of seconds.

In chapter 1, we review past studies on fluid mechanics related to swimmers at interfaces. Pushers, such as bacteria and sperm, have been observed to be attracted by solid surfaces, and such behaviors were analyzed by many researchers. Ciliated colonies *Volvox* were observed dancing with one another when they are close to a solid surface. Crowdy

et al. (2011) have studied the crawling of a water snail below the water-air interface. The crawling was explained by the deformation of the interface, which may not appear for microorganisms. No studies related to the motion of a single microswimmer close to water-air interfaces has been performed. In this study, we first characterize the entrapment of ciliated microswimmers at the water-air interface, we then clarify the mechanism of entrapment, and finally we investigate the collective motion at the interface.

In chapter 2, we characterize the entrapment of *Tetrahymena thermophila* at the water-air interface, and we experimentally investigate the mechanism of this entrapment. We observed a sudden drop by 70% of the swimming velocity when the cells are getting at the interface. They also regain their swimming velocity instantaneously when escaping from the interface. In order to evaluate the effect of geotaxis, aerotaxis, and surface tension on the entrapment, the cells were exposed to different experimental conditions. Even though the negative geotaxis and positive aerotaxis lead to the aggregation of cells below the water-air interface, we have found that they are unrelated to the mechanism underlying behind the entrapment itself. On the other hand, the addition of surfactant in the medium revealed that interfacial physics has an important effect on the entrapment since the number of cells trapped at the interface suddenly dropped to zero when enough surfactant was added. We thus concluded from the experiments that the entrapment is mainly governed by surface physics.

In chapter 3, we developed a mathematical model in order to clarify the mechanism of the entrapment. *T.thermophila* is modeled as a squirmer and the motion is analyzed using boundary element method. We applied two kinds of boundary conditions at the interfaces to represent the WAI and the solid wall, i.e. a stress-free surface and a no-slip surface. In the case of stress-free interface, it takes more time for the squirmer to orientate away from the interface than in the case of the interface with no-slip boundary condition. The

mechanism can also be explained by the lubrication theory. Therefore we concluded that the entrapment is due to the stress-free boundary condition that only exists for fluid-fluid interfaces such as water-air interface.

In chapter 4, we investigate the characteristic of the collective motion of *T.thermophila* at the WAI. By calculating the pair correlation function, the velocity correlation and the orientation correlation, we found that the motion of the cells is correlated over about 2 body lengths (4-5 body widths). The correlations were slightly affected by surface concentration of cells. We have also observed for the first time, to our knowledge, the collective motion of neutral swimmers in a biological system, though it was not predicted by former theories. Moreover when the surface is stress-free, and the initial angle relative to the surface is steep enough, the cell is even trapped at the interface. It is remarkable to see that the nature of the collective motion of these cells is different from the collective motion of bacteria for which the motion is correlated over the tenths of body lengths. We think the difference in the collective motion comes from whether the cell is a pusher or a neutral swimmer.

In this study, we report for the first time the existence of the entrapment at the water-air interface of a swimming ciliated microorganism as well as the collective motion of neutral swimmers in a biological system. We also have clarified the mechanism of this entrapment as a consequence of the stress-free boundary condition found at the water-air interface. These finding are important to understand cell biology and the transport phenomena at WAI.

Acknowledgements

French student in fundamental physics, I always had some sort of interest towards biology too... And I was also quite curious about how would be a life in Japan.

To have allowed me to access both of these wishes, I'd like to to show my gratitude towards:

* Professor Ishikawa Takuji, my PhD supervisor. Not only did he gave me the possibility to perform my PhD in the PFSL laboratory but he also helped me to settle when I first arrived in Sendai, away from any familiar face. I feel particularly lucky to have been able to do research under the supervision of a person so enthusiastic about science, and who always showed me the way in my topic when I wasn't sure of the next steps. I'm honored to be his first PhD student.

* Professor Takami Yamaguchi, the head of the laboratory, who gave me financial support during my thesis, helped me to rent a new flat when I came back after the disaster that stroke Japan the 11^{th} March 2011. He always considers each and every student equally, he arranges the most convenient conditions of work, and even give to all of us the opportunity to participate to exiting international conferences.

* Professors Hironori Ueno and Keiko Numayama-Tsuruta who taught me how to handle biological objects and how to use microscopes. They helped me sometimes with my experiments, and answered to lot of my questions even in the middle of the night, at times we were together at the laboratory at such hours.

* Professor Yohsuke Imai who gave me on multiple occasions advice on writing reports

and fellowship applications. Thanks for the ride to the hospital too.

* Professor Jean Cohen without whom I wouldn't have discovered the fascinating world of ciliated microorganisms.

* Professors Roland Mastripolito and Benoit Ladoux for creating the master of interface physics/biology.

* Doctor Davide Giacché for the laughers and the chats mixed with some advice about life.

* The secretaries of the laboratory who greatly helped me with the japanese red tape while being patient and efficient all at once. I'll never forget their good mood. And thanks for letting me play with professor Yamaguchi's dog from time to time.

* The awesome students of the PFSL laboratory, and in particular Daiki and Take-chan for their help and cakes.

* Professor Yamaguchi's wife, Ms. Uiko Yamaguchi who has jovial talks with the students during the parties of the laboratory.

* Mr. Gregor Burdeos with whom I had interesting discussions about cellular biology.

* All of my friends for giving me motivation and making my life and work more enjoyable, and in particular Julien and Buddy-kun.

* My parents and younger sister who supported my choice to go to such a far and foreign country such as Japan, even after the disaster of March 11.

* My dear azizam for her love and support during my redaction. Alz reehari.

* The Ministry of Education, Culture, Sports, Science and Technology of Japan (MEXT), Global COE program, Japan Student Services Organization (JASSO), Tohoku Kaihatsu Kinen Zaidan and Aoba Foundation for the Promotion of Engineering for supporting me financially.

Contents

Chapter 1

Introduction

Beneath the air surface of the oceans and lakes is a microlayer that tends to accumulate partly hydrophobic particles and organic molecules as well as microorganisms [8, 9]. The study of organisms in the bulk below the water-air interface (WAI) is usually called neustolonogy [10], which in more recent studies lead to the investigation of the physics behind the interaction of microorganisms with this interface [11]. The presence of such organisms seems to have a wild scale of effects on the surrounding environment. It has been reported that these organisms can affect the rate of gas exchange between the air and water [12]. The presence of bubbles in natural environment tend to put some of these microorganisms (dead or alive) in suspension in the air [13, 14] possibly affecting the meteorology [15, 16] and, in case of pathogen microorganisms, possibly being responsible for diseases [17]. Consequently, the understanding of the behavior of microorganisms close to the WAI is fundamental to understand how we should interact with the environment.

The understanding of the interaction of cells at fluid-fluid interfaces is also of high interest in medicine. In the past years, some groups have been concentrating their effort into trying to unravel the mechanism behind mucous transport in trachea generated by ciliated epithelial cells, namely muco-ciliary transport process. But the experimental modification of the physical properties of the two phases concerned by this process, mucus layer and lower periciliary layer, being difficult, study mainly concentrated on simulation work [18, 19]. By using the natural ability of ciliated microorganisms to be trapped at fluid-fluid interfaces, we could experimentally verify how cilia interaction with such interface, and

experimentally study the effect of physical properties of the fluids on this interaction.

Even though many of these studies have been concentrating on cells in the bulk below the water-air surface, only Nicola Ricci, in an unrelated work about the ethology of ciliates [20], mentioned how in one of its stages Oxytricha bifaria is "creeping" at the velocity of 220 μm.$^{-1}$ at the WAI while creeping at 550 μm.$^{-1}$ on solid substrates. It therefore seemed interesting to study the behavior of ciliates at the WAI itself and not only in the bulk below.

1.1 Experimental background

1.1.1 *Tetrahymena thermophila*

Biological overview

T.thermophila is a fresh-water unicellular eurakyotic cell. Its drop-like shaped body is covered with cilia, figure 1.1 [21], which most of them are used for swimming. The ellipsoidal body has an aspect ratio of two with a short axis of 25 μm and a long axis of 50 μm. Most of the cilia are $\sim$5 μm long except for a zone used for endocytosis, called oral apparatus, where the cilia are twice as long [22]. The cilia covering its body move in a coordinated fashion called metachronal wave. They are then beating in a spatial and temporal periodic motion.

This ciliated cell has the advantage of being cultivated in bacterial rich environment as well as bacterial free environment. This allows then to avoid possible chemical interference due to the presence of bacteria or on the contrary to use bacteria as vessel for interference RNA. As many other bottom heavy ciliated cells, when their concentration is high enough they form bioconvection patterns.

This is one of the peculiar cell with two nuclei, a micronucleus used to store all the genetic information and a macronucleus from which the cell actually read the genetic information. It also has two methods of reproduction, figure 1.2. In food rich environment, the cell goes through mitosis while, when deprived of food, it pairs with another cell, exchange their small nuclei in order to mix their genetic code and form new macronuclei more favorable for the new environment. It also possesses human-like genes related to

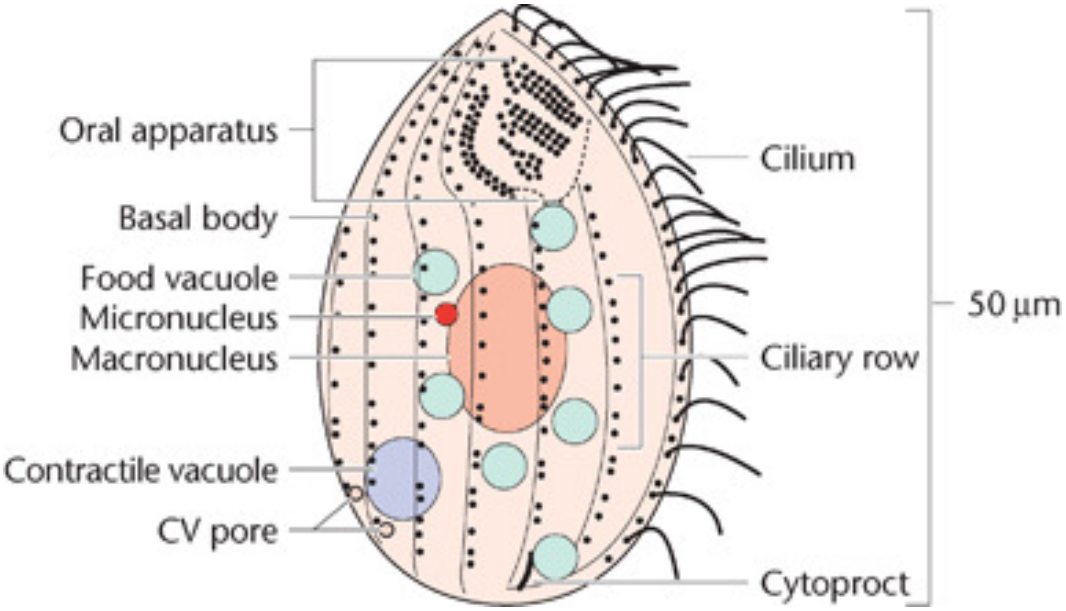

Figure 1.1: Representation of *Tetrahymena thermophila* [21]

cilia, making it convenient to study the expression of some of human genes.

Taxes

As many organisms, *T.thermophila* is subjected to different taxes such as geotaxis, aerotaxis, galvanitaxis, chemotaxis, and so on. In this study, we took into account two specific taxes since they could be responsible for the formation of a bulk below the water-air interface: the positive aerotaxis and the negative geotaxis.

The negative geotaxis means that the cells tend to swim in the opposite direction of the gravitational field. It is easy to understand how the cells are compelled to swim upward when taking into account their bottom heaviness. As shown in the figure 1.3, the center of mass and the center of geometry of the cell are different. In addition, the gravitational force f_g is applied on the center of mass and directed downward, while the buoyancy force f_b is applied on the center of geometry and directed upward. These two forces of opposite direction and applied on two distinct points on the cell create a torque

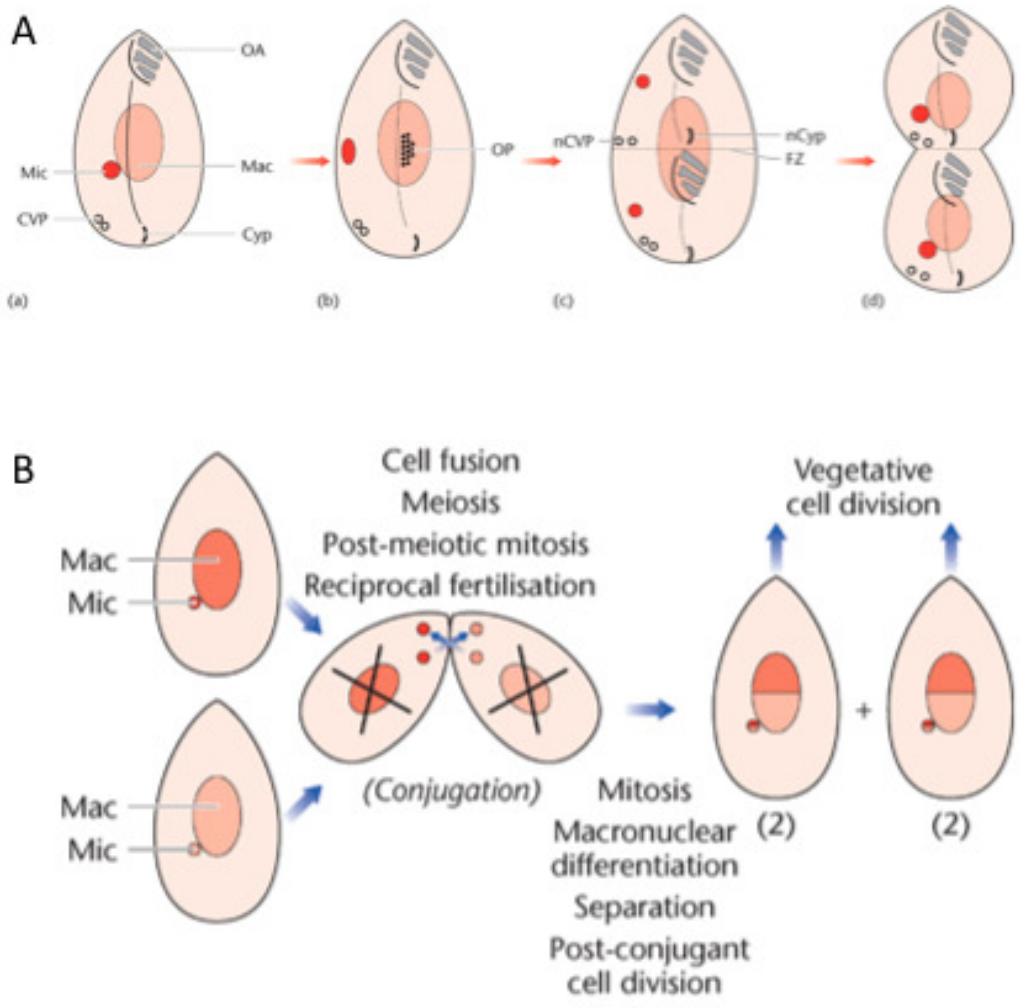

Figure 1.2: Sexual cycle of *Tetrahymena thermophila*. (A) Asexual reproduction. (B) Sexual reproduction. [21]

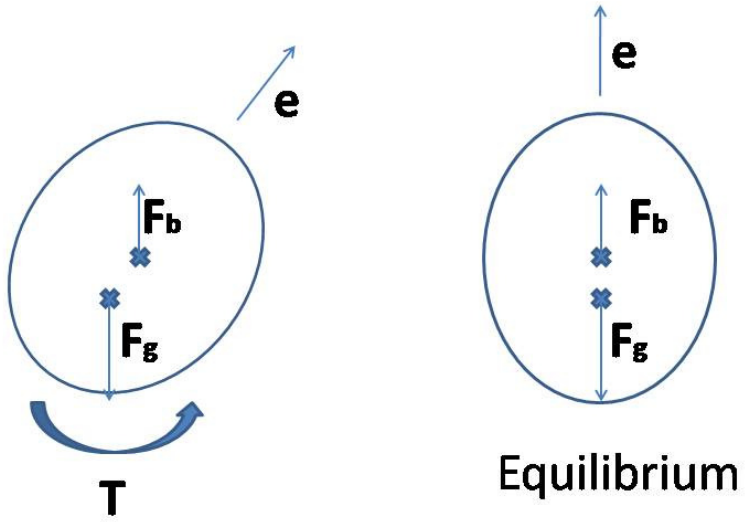

Figure 1.3: Negative geotaxis principle. The torque orientates the cell upwards, therefore making it swim globally upwards. **e** is the vector orientation of the cell, $\mathbf{F}_b$ is the buoyancy force. $\mathbf{F}_g$ the gravitational force and **T** the torque that is applied on the cell by the two later forces.

that tends to orientate the cell upward and globally makes it swim in the opposite direction of the gravitational field.

The positive aerotaxis means that the cells tend to swim towards higher gradient of oxygen.

Cilium structure and motion

As shown in figure 1.4(A) [21], the cilium has two phases during one cycle of beating.

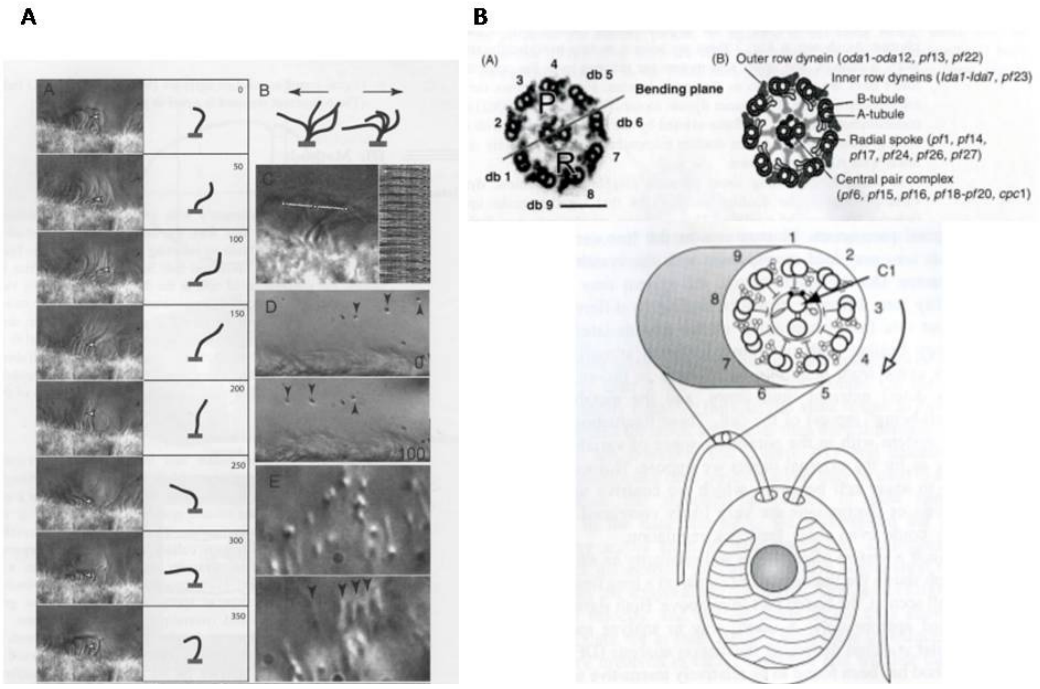

Figure 1.4: (A) Motion of a cilium. (B) Structure of a cilium. [21]

The effective stroke, in the normal plane to the cell wall while being strait, allows a large drag force on the full length of the cilium. And the recovery stroke, in the same plane, beat in the opposite direction of the previous stroke but bends so to lead to a drag of a lower intensity than the effective stroke. These two different strokes when averaged in time, lead to a globally non-zero thrust force which allows the cells to move forward or backward depending on the direction of the strokes.

Figure 1.4(B) [21] shows the structure of the cilium itself. It is formed of nine doublet microtubules surrounding two central singlet microtubules. These double microtubules are made of an A-tubule and a B-tubule and linked to the central microtubules by radial spokes. Each doublet microtubule is linked together with Nexin-link. Figure 1.5 represents how Dynein-tail is fixed on the A-tubule, and the stalk interacts with the neighboring doublet microtubule depending on the nucleotide. The dynein molecules induce microtubule sliding and make bending motion. Since the cell can control the bending the ciliary bend-

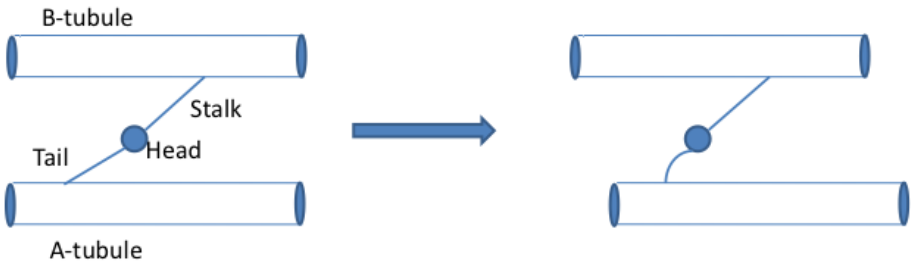

Figure 1.5: Mechanism of the sliding between doublets induced by dynein action.

ing form, fluid flow is generated around the ciliary motion. Hence we can assume a model of a force shell such as the one used in chapter 4.

1.1.2 Fluid-fluid interface

Interfacial tension

When two different phases are in contact with each other, the molecules at the interface experience an imbalance of forces. However as molecules tend to stay together, an accumulation of free energy appears at the interface to keep the cohesion of non-miscible particles at the interface. This energy manifests itself as a contracting force per unit length that will prevent external body (gas molecules, liquid molecules or solid bodies) to interact with the molecule inside the bulk.

This phenomenon can be seen easily when a droplet is hanging from the faucet. Difference of pressure with the ambient air (the lower one) and the pressure inside the water (the higher one) is compensated by the deformation of the water into a droplet, fig. 1.6. Without such force the water molecules would simply spread in the air instead of staying together in a liquid phase. The surface tension γ is defined as $\Delta P = \gamma\left(\frac{1}{R_1} + \frac{1}{R_2}\right)$ with R_1 and R_2 the local curvature in normal direction to each other and ΔP the difference of pressure in the two phases.

When a liquid is in contact with a solid substrate, the interfacial tension will shape the liquid into a droplet in order to minimize the area of contact between the liquid and the solid substrate in regard of how "easy" (that is, low energy costing) are the interactions between the molecules in the medium and the molecules composing the solid substrate.

Surfactant

Surfactant molecules are molecules that can lower the interfacial tension. They are composed of both a hydrophobic and a hydrophilic part as shown in figure 1.7(A). Thanks to these two properties the surfactant can easily interact with aqueous material as well as non-aqueous material, creating a chemical bridge being these two materials that reduces the difference of energy at the interface. The surfactant can somehow coat, with its hydrophobic part, non aqueous material entering an aqueous phase while the hydrophilic part allows an easier interaction between this complex and the water, figure 1.7(B).

Apart from reducing the surface tension, the surface has other effects on the liquid, among them, is the Marangoni effect. The Marangoni effect in itself appears when there is a gradient of surface tension at an interface. As explained above, the surface tension

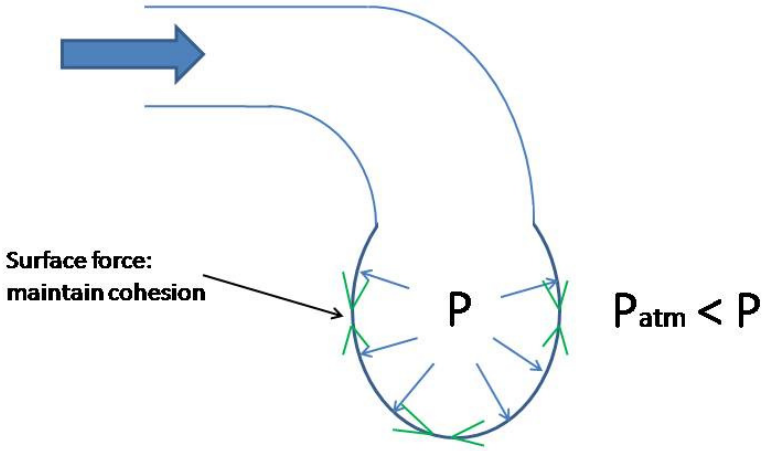

Figure 1.6: Thanks to the surface tension the molecule of water stay together instead of spreading in the air.

being a cohesive force that pulls together the liquid at an interface, an area of stronger surface tension will pull more strongly the liquid at the interface. Therefore a flow from the region of lower surface tension to the region of higher surface tension will appear. As shown in figure 1.8, when there is a gradient of surfactant at the interface, a gradient of surface tension also appears inducing therefore a flow that will homogenize again the repartition of surfactant at the interface.

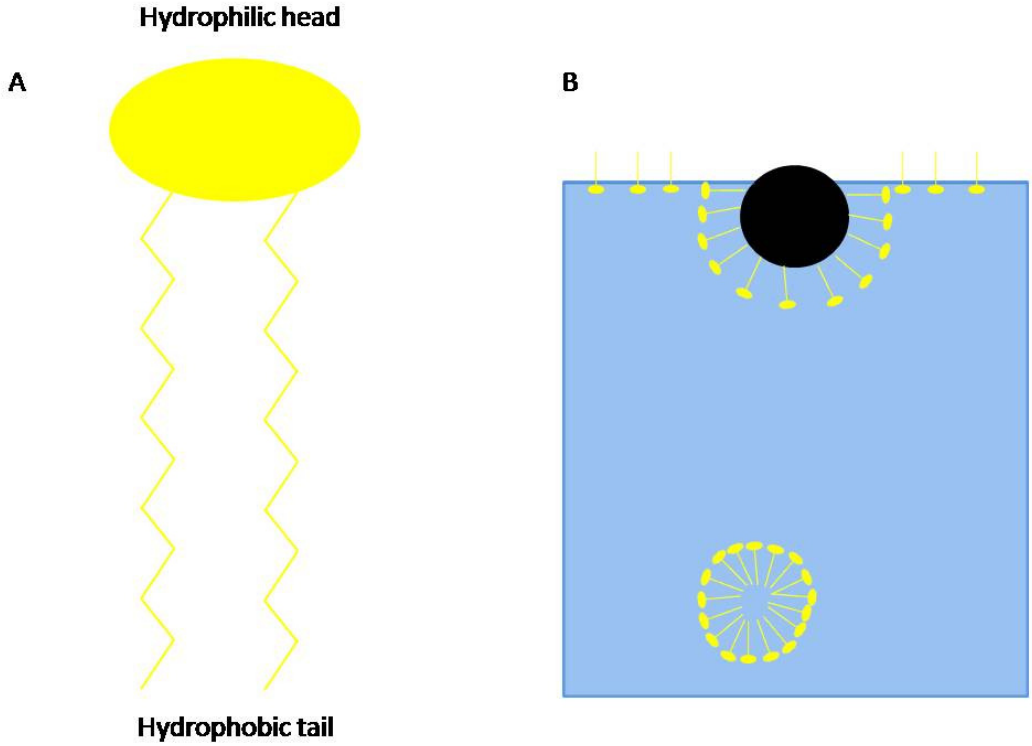

Figure 1.7: (A) Structure of a surfactant. (B) Surfactant in water and its interaction with a hydrophobic body.

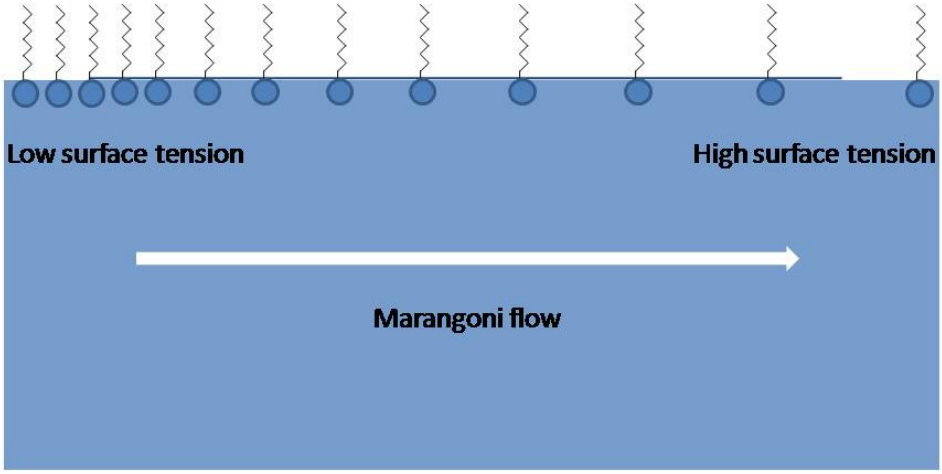

Figure 1.8: Marangoni flow due to a gradient of surfactant.

1.2 Theoretical background

1.2.1 Modeling of ciliate

Squirmer

The squirmer model was first developed by Lighthill [23], and then extended by John Blake in 1971 [24]. The main idea was to represent the ciliary motion as an envelope, figure 1.9(A), above a solid sphere with no slip condition on its wall. The envelope was defined as if joining the tips of the cilia, and can be deform in the azimuthal and radial direction. In order to represent the propagation of the metachronal wave, he defined the motion of the envelope as a superposition of a non-trivial number of radial waves and of tangential waves which individual characteristic are time dependent, equation 1.2. It is found that the direction of propagation of the transversal waves defines the direction of propulsion as shown in figure 1.9(B) [24].

$$R = a\Big[1 + \epsilon \sum_{n=2}^{N} \alpha_n(t) P_n(cos\theta_0)\Big], \qquad \theta = \theta_0 + \epsilon \sum_{n=1}^{N} \beta_n(t) V_n(cos\theta_0) \tag{1.1}$$

It would also appear that the first order of the velocity is sufficient to justify the fact that the squirmer is moving while the second order is necessary to have the stress field generated by a solitary squirmer. Therefore, in most of numerical studies, it is common to consider only the first 2 orders of the tangential velocity to have an accessible calculation time-scale [25]. The velocity field is then simplified to equation 1.2.

$$u_\theta(\mathbf{r}_s, \mathbf{e}) = \sum_{n=1}^{2} \frac{2}{n(n+1)} B_n\big(\frac{\mathbf{r}_s.\mathbf{e}}{a}\frac{\mathbf{r}_s}{a} - \mathbf{e}\big) P_n'(\mathbf{r}_s.\mathbf{e}/a) \tag{1.2}$$

with $\mathbf{r}_s$ the point on the surface of the envelop, $\mathbf{e}$ the unit orientation vector of the swimming of the squirmer, a the radius of the squirmer.

From this velocity field, is it usual to categorize the squirmer into puller, pushers, and neutral swimmer, fig. 1.10 [26]. The behaviors of such swimmers are quite different. An example of this as been illustrated by Llopis [27], where it is shown that a puller swims away from a solid wall, while a pusher swims towards it.

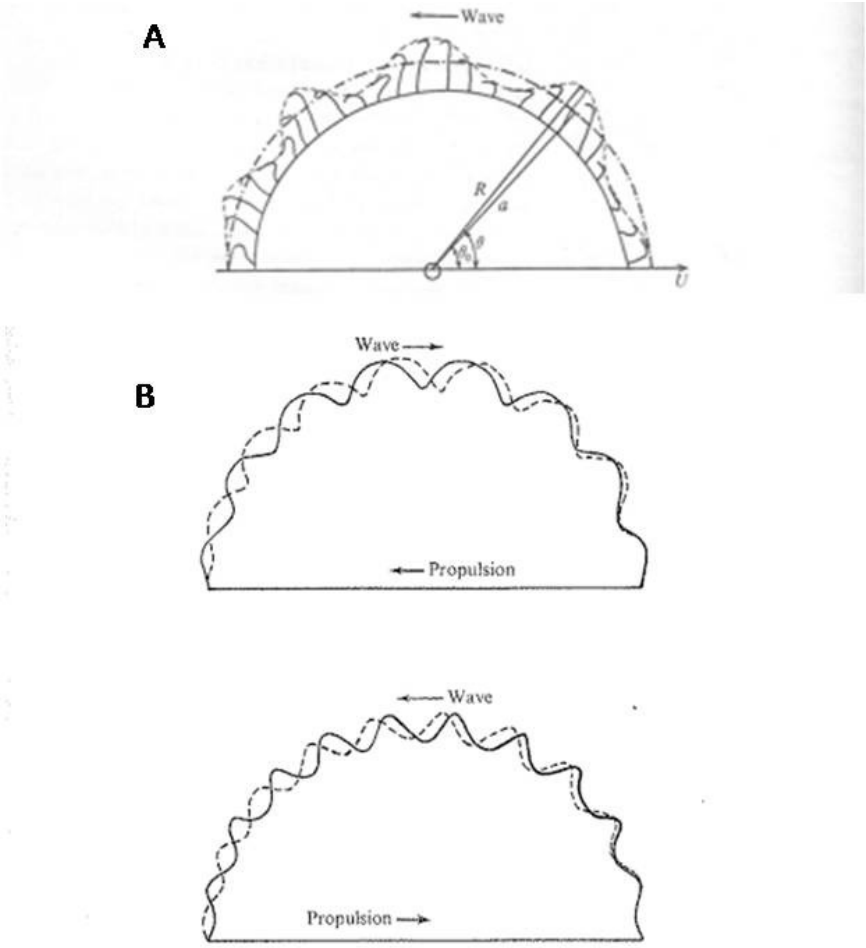

Figure 1.9: (A) Envelope linking the tips of the cilia together. (B) The wave propagation determines the propulsion direction. [24]

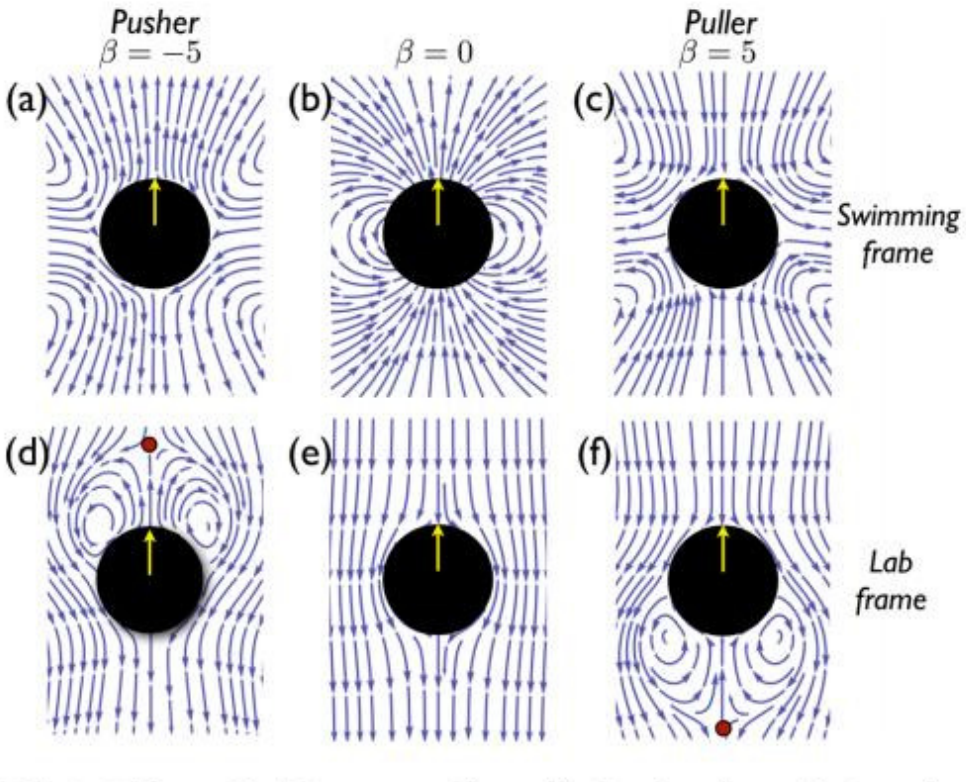

Figure 1.10: Three type of squirmers, and their associated flow field [26]. β is a parameter related to the type of swimming. If positive the swimmer is a puller, if negative it's a pusher, and for neutral swimmer $\beta = 0$

1.2.2 Interfaces theories

Method of images

The method of images comes from the uniqueness theorem, which states that an object satisfying a given set of conditions or properties in a system defined by linear equations is the only such one that exists. It's a mathematical tool to define a new system satisfying the boundary conditions imposed by the initial system, with respect to a plane of symmetry, in order to facilitate the resolution of the initial problem. In order to give an example of this method, instead of using fluid mechanics, let's use electrostatics. As shown in figure 1.11(A), let's consider a particle q charged positively at a distance r from an infinite wall. At the wall the electric field is assume to be zero ($E_w = 0$). Then, when trying to solve the electric field of a charge close to a wall, we have to integrate the Gauss's law $\nabla.\mathbf{E} = \frac{\rho}{\epsilon_0}$ (ρ being the electric charge density and ϵ_0 the electric constant in void), while taking into account that $E_w = 0$. Such a system needs more mathematical calculus than the one shown in figure 1.11(B). In the second case by adding an imaginary particle negatively charged on the symmetric position to the wall, we obtain the same condition on the wall, but the calculus is simplified as it becomes the sum of the electric field of these two charges if they were alone in void but at the same position as in the later system. Using such ideas and being allowed to do so in the case of Stokes flow (liner system), Blake [28, 29] determined the flow field and stress field of a point force close to a solid wall and a stress free interface by defining the Green function in the case of the wall 1.3, and in case of the stress free interface 1.4.

$$J_{ij} = \frac{1}{8\pi\mu}\left[\left(\frac{\delta_{ij}}{r}+\frac{r_i r_j}{r^3}\right)-\left(\frac{\delta_{ij}}{R}+\frac{R_i R_j}{R^3}\right)+2h(\delta_{j\alpha}\delta_{\alpha k}-\delta_{j3}\delta_{3k})\frac{\partial}{\partial R_k}\left(\frac{hR_i}{R^3}-\frac{\delta_{i3}}{R}-\frac{R_i R_3}{R^3}\right)\right] \tag{1.3}$$

$$J_{ij} = \frac{1}{8\pi\mu}\left[\left(\frac{\delta_{ij}}{r}+\frac{r_i r_j}{r^3}\right)+(\delta_{j\alpha}\delta_{\alpha k}-\delta_{j3}\delta_{3k})\left(\frac{\delta_{ij}}{R}+\frac{R_i R_j}{R^3}\right)\right] \tag{1.4}$$

with i, j spatial coordinate indices, $\alpha = 1, 2$; $\mathbf{r}$ is the vector between a point in the liquid and the point force: $\mathbf{R}$ is the vector between the same point in the medium and the symmetric image of the point force in regard of the solid wall.

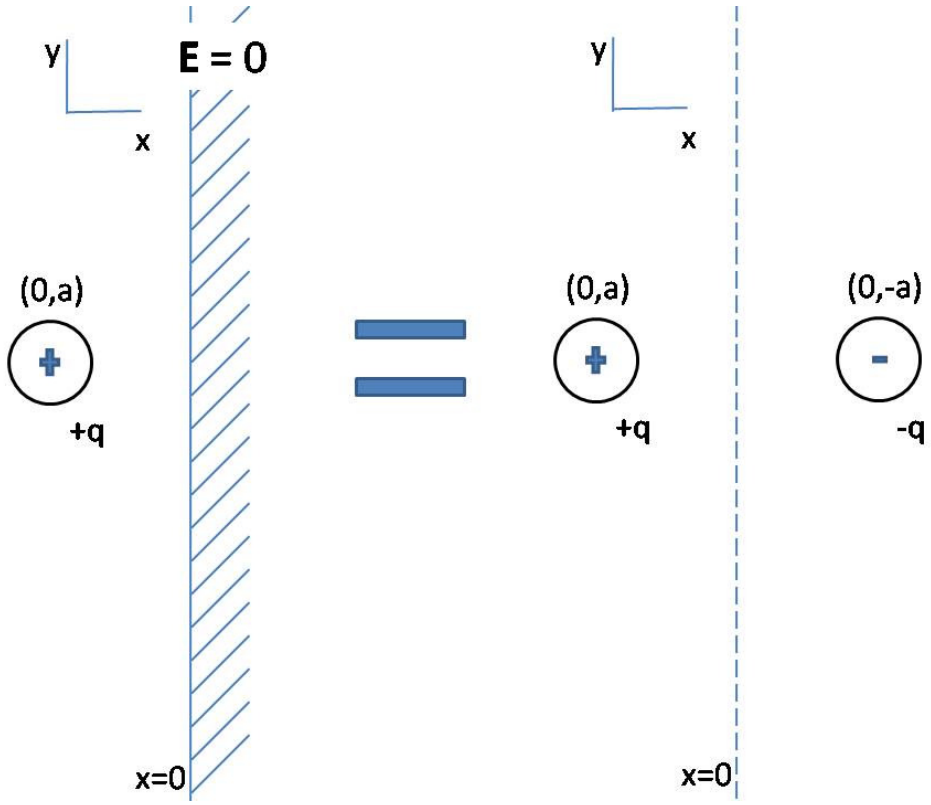

Figure 1.11: (A) Initial system with one particle and a wall. (B) Mathematically equivalent system.

1.2.3 Previous related studies

Experimental studies

In the previous works, the behavior of microorganisms has been reported when moving close a solid substrate for ciliated as well as for flagellated cells. The most common works were performed on the case of dancing Volvox [5], on the case of the coordinated motion of spermatozoa close to a solid wall [30] and for the motion of a bacterium close to a solid wall [7].

Volvox is a spherical bottom heavy colony of flagellated and non-flagellated algae. Depending of its age, the size of the colony will be different and their swimming behavior changes. When young, these colonies rotate on themselves and tend to swim only upward

in absence of an external flow and light. they are yet not too dense which allow them to have a thrust force larger than the gravitational force, and they are therefore swimming upwards. When older, the colony is bigger but essentially composed of non-flagellated cells, therefore the thrust force is not efficient enough to prevent *Volvox* from sinking. In the case of young *Volvox*, it has been observed that as they gather on the upper part of the liquid close to the cover slip, the colonies are pairing into a Waltz which can be explain by the specific flow created, figure 1.12(b) [5], when a colony is close to the cover slip. Such flow tends to make the colonies attract each other and the rotation of the colonies induces a global torque on the global system composed by the two colonies, making the colonies turn around each other. But the youngest *Volvox* colonies are not the only ones dancing. It appears that the old colonies, on the bottom of the fluid close to the microscope glass are performing a minuet. In this case the dance is due to the presence of one colony above another that is moved and tilted in one direction by the rotation of the other below, but stabilized itself on the other side of the colony thanks to its bottom heaviness, and is therefore once again moved on the other side while being tilted.

The sperm cells of sea urchins have been reported to form clusters of about 10 spermatozoa swimming in circle while staying together and synchronizing the frequency beating of their flagella. These clusters were periodically arranged at the solid wall as shown in figure 1.13 [30]. It would appear that even though the pattern was preserved, the clusters were diffusing ten times faster than rings of the same size at the same temperature would have diffused. By considering a simple model of sperm cell being represented as particles with the diffusivity of the cluster and submitted short-range attraction and long-range repulsion, the same periodic repartition of circular clusters was found [30].

The motion of a single bacterium has been reported and modeled many times. A three dimensional reconstruction of the bacterium trajectory from experimental tracking, figure 1.14 shows that when the bacterium is getting close to a solid wall, it tumbles less often and tends to swim parallel to the wall, with sometimes a rotational trajectory. In his work, Davide Giacché [4] shows that such a behavior can be explain by hydrodynamic interactions and the distance of the cells to the wall depends notably on the wave number of the beating of the flagellum.

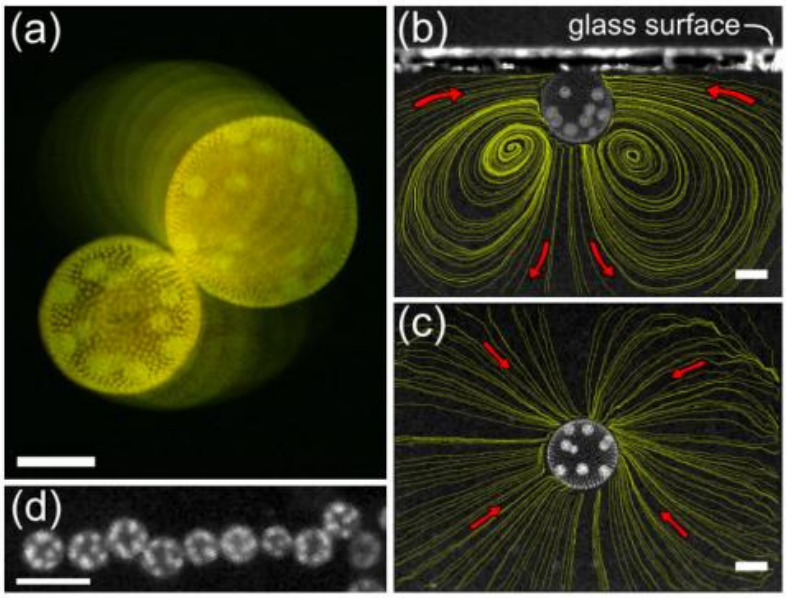

Figure 1.12: *Volvox* behavior close to a cover slip and flow field generated by a single colony. [5]

Numerical study

In his work [31], Saverio Spagnolie represents microorganism as force dipole, source dipole, or force quadrupole. In all cases, apart from the case when they simulate a pusher, the model swimmer is swimming away from a solid wall even when it's directed towards it as an initial condition. On the contrary the pushers like parameters lead to a case where the wall attracts the swimmer.

Darren Crowdy [32] considers the case of the stress free interface for a water snail crawling underneath the water-air interface. In order to represent numerically this snail, he considers a swimmer as a non-rotating tread milling circular motion, and represents it as an effective singular point by superposing potential quadrupole and dipole contribution. He has found that one of the necessary boundary condition to obtain a steady motion of such singularity close to the interface is to consider the interface to locally deform above the singularity so that the orientation of the swimmer doesn't change. Using such conditions and swimmer he could obtain the same crawling as the water snail with a steady motion.

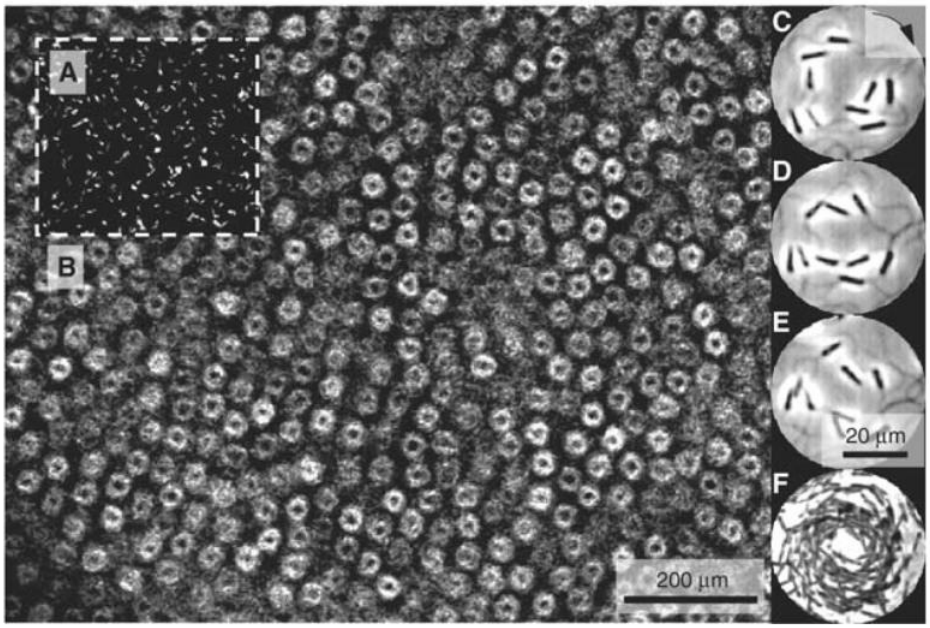

Figure 1.13: Pattern formation of sperm cells close to a solid wall. [30]

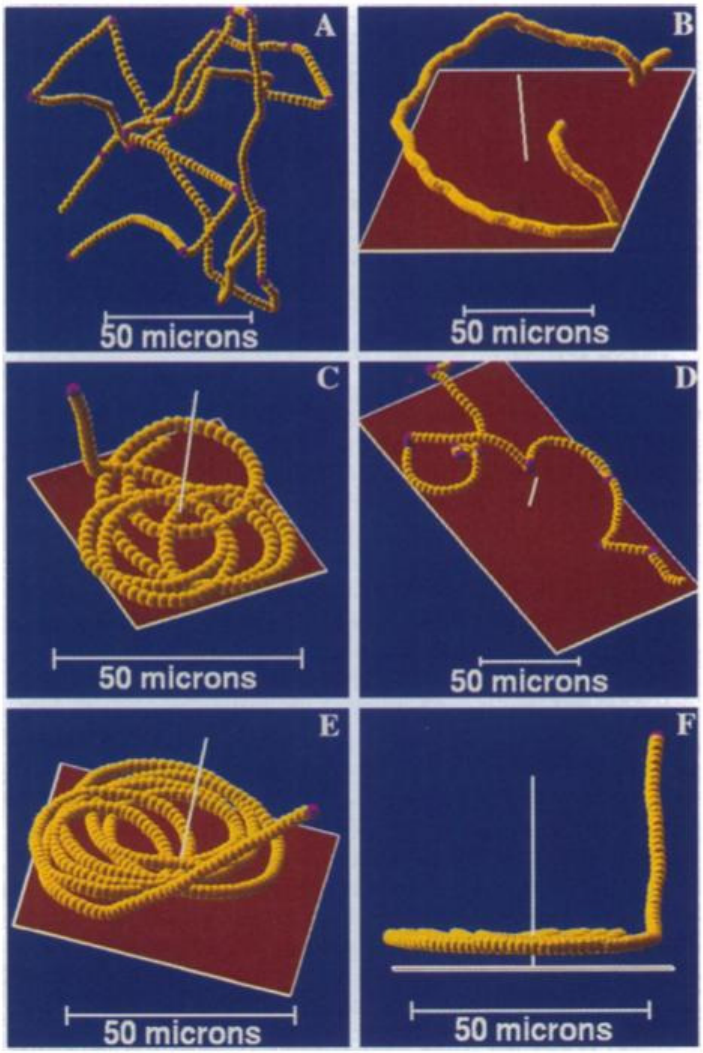

Figure 1.14: Trajectories of a bacterium away from a wall (A) and close to a wall (B-F). [7]

1.3 Purpose of the study

It has been established that the existence of microorganisms close the WAI has a wide range of consequences, such as the chemistry of the medium, the spreading or prevention of disease and therefore many studies have been conducted on the relation between interfaces and micro-organisms from biological as well as physics point of views.

However, in previous works, the accumulation of microorganisms below the WAI has been mostly attributed to biological causes, only considering the accumulation at the very interface in case of the formation of biofilm. Even though it has been briefly reported the creeping of a ciliated creepers at the WAI, the possibility of swimming ciliates at the interface itself has been overlooked to our knowledge.

In this study, we thus investigate the entrapment of *Tetrahymena* at the WAI by characterizing it, and by clarifying the mechanism behind it. We also investigate the collective motion of these cells at the interface, and we compare it to former finding of bacterial coherent structure.

1.4 Structure of the thesis

In the remaining of the thesis, the investigation of the behavior of cells at the WAI will be reported as follow: Chapter 2 is the confirmation of the entrapment phenomenon of *Tetrahymena* at the water-air interface, its consequence on the swimming of the cell as well as a first experimental investigation of the mechanism behind the entrapment. Chapter 3 is the first step of the theoretical as well as computational investigation, by explaining the entrapment from the viewpoint of hydrodynamics. Chapter 4 reveals the generation of collective motion after enough days in the set-up where the cells were cultivated. And lastly chapter 5 presents the conclusion and prospects.

Chapter 2

Experiments: Characterization of the entrapment and investigation of leading mechanism

2.1 Introduction

Even though the formation of biofilm at the water-air interface has been widely investigated in the past studies [33], notably how surfactants affect the formation of biofilms [34], no report of the accumulation of swimming ciliates at the interface itself has been reported to our knowledge. In this chapter, I will first characterize the entrapment of *Tetrahymena thermophila* at the surface by comparing the swimming velocity and number of cells at the interface with those inside the medium, which is away from any interfaces. Secondly I will present the investigation of the possible causes of the entrapment by looking at the effect of the taxes and surface properties of the interface on the entrapment, before presenting how the ciliary motion is affected by the presence of the interface.

2.2 Method

Tetrahymena thermophila, wild type: CH1, were cultivated at 27°C in PYD medium, that is an aqueous solution composed 1% of protease peptone, 0.5% of yeast extract and 0.87% of glucose in pure water. 20μl of stock cells were added to 8ml of sterilized PYD in a circular petri dish with a diameter of 60 mm and a depth of 15 mm. They were multiplied for 6 days before being inoculated again in the same manner in a new petri dish. Only the cells from the second inoculum would be used either from day one to day seven, or at day five only.

In order to observe the behavior of the cells at the water-air interface during the course of seven days, and while adding surfactant in the medium containing cells at day 5, we used the set-up shown in figure 2.1(A). 1 ml of medium containing cells was poured in a PDMS pool of 25 mm of diameter and 2 mm of depth. To avoid evaporation, we obtained a 100% humidity condition by enclosing the pool in a circular petri dish with a diameter of 60 mm and depth of 7 mm. Creating the closed space also allowed us to avoid the effect of air flow on the cell motion at the water-air interface. PDMS was used since it is biologically inactive and once hardened it doesn't modify the physical property of the fluid. In order to make this pool, we manufactured the mould as described in figure 2.1(B), poured the freshly made PDMS in the mould, and after removing the air bubble with desiccator method, we let it harden for 1 hour at 80°C in a dry heat sterilizer. For the observation of the behavior of the cells at the water-air interface, after pouring the cells in the pool, the petri dish was placed under the upright phase contrast microscope (Leica, DM 400B, Germany) using the 10 times objective lens (Leica, HCX PL FLUOTAR 10x/0.30 PH1, Germany) for 10 minutes to let the time to the cells to reach a "stable state" in the pool. In the first minute after pouring them, more cells are trapped than later, even though the later state doesn't change afterwards. For each type of experiment six different samples inoculated at three different days were used.

The surfactant used was Tween 20 (KWH506, Wako, Japan). The surface tension was measured by a Wilhelmy plate method using automatic surface tensiometer (DY-300, Kyowa, Japan). In case of the natural culture fluid, the surface tension slightly varies within the time scale of the measurement. Here, we measured the static surface tension for one minute, so that the value is sufficiently stabilized as shown in figure 2.2.

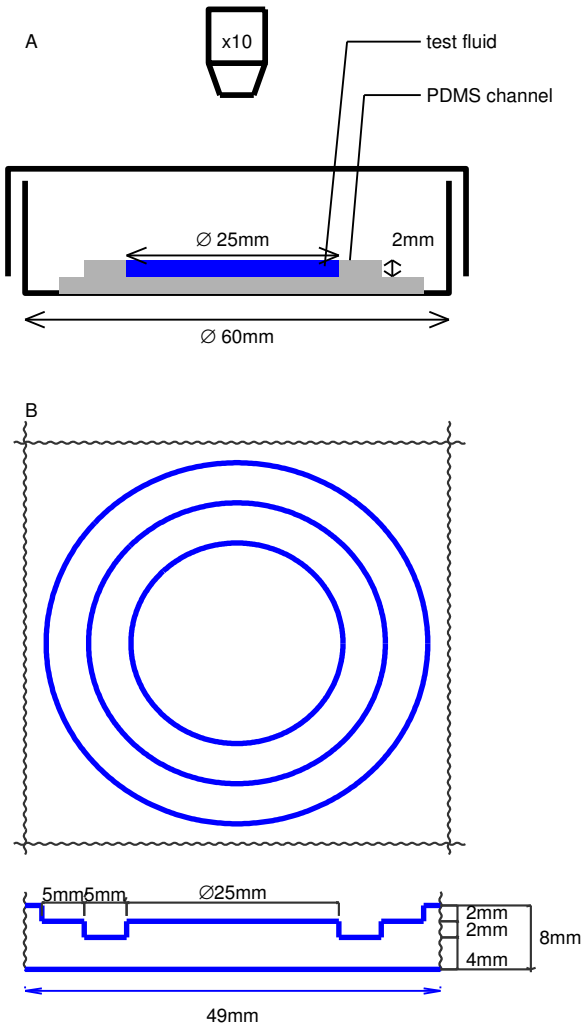

Figure 2.1: (A) Set-up used in order to observe the change of behaviour of the cells over the course of seven days, and when adding surfactant. (B) Aluminium mould used to make the PDMS pool used here.

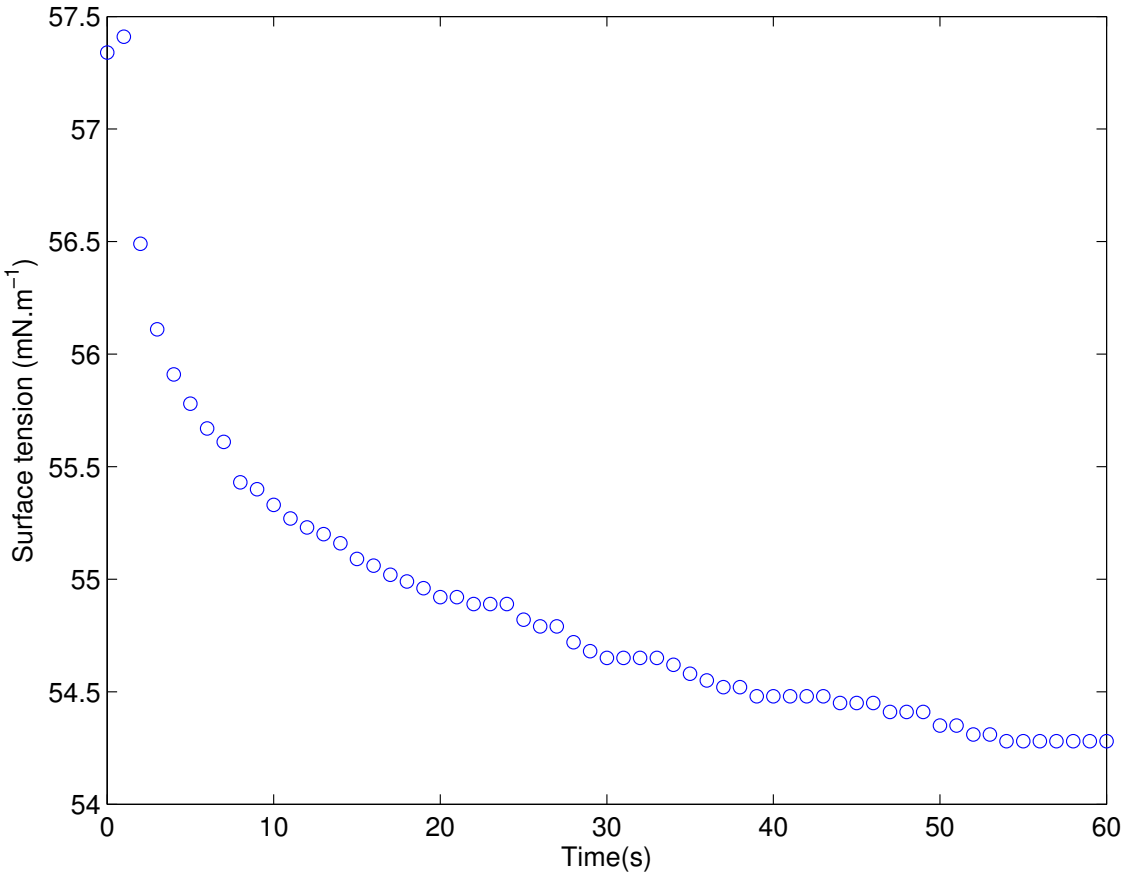

Figure 2.2: Example of the measure of the surface tension of the culture over the course of one minute.

Table 2.1: Protocole of dilution used over the course of seven day to count the number of cells with the plankton counter.

Time (days)	1	2	3	4	5	6	7
% of medium with cell in formaldehyde	91	83	30	5	5	1	1

The cells' motion at the interface and inside the medium, which is away from any interfaces, was recorded by using the CMOS camera (Basler A602fc, Germany) at 30 fps in a window of 570 μm $\times$ 430 μm. The trajectories were manually extracted from the movies using the plugin MTrackJ of ImageJ (http://rsbweb.nuh.gov). When the medium was diluted, two samples of the same day after inoculum were used to obtain the dilution. The first one was centrifuged five minutes at 300 rpm in order to obtain the medium without cells but with the same chemical composition as the second one. And the centrifuged solution was then added to the sample still containing cells low enough to avoid hydrodynamic cell-cell interactions, but in order to obtain a concentration high enough to easily record cells at the interface. To obtain the velocities of swimming cell away from any interfaces, only the trajectories of cells staying in the plane of focus were extracted. The surface concentration of cells was calculated from pictures taken also using the CMOS camera. Five pictures were taken around the pool for each sample. The surface value of each sample was first calculated by taking the mean value of the five pictures, and then the mean value of the six samples was calculated and considered as the surface concentration of the considered day in the defined condition of the experiment. Lastly, to calculate the concentration of cells in the medium, they were diluted in formaldehyde, in the proportions described in the table 2.1 (e.g. 10% means 100 μl of medium with cells is poured in 900 μl of formaldehyde), to fix the cells and facilitate the counting. After mixing, the fixed cells were poured in the plankton counting plates (Matsunami, Japan). The mean value of the concentration of the six samples was then calculated. The standard deviation for the different quantities described above was defined by the equation 2.1.

$$\left(\frac{1}{n}\sum_{i=0}^{n}(x_i-\bar{x})^2\right)^{\frac{1}{2}} \tag{2.1}$$

The set-up used to observe the behavior of the cells in the three conditions to verify

the effect of the geotaxis and chemotaxis on the entrapment is relatively the same as before except for some details. First of all, for this experiment 120 μl of medium containing cells was poured in a PDMS pool of 8 mm of diameter and 2 mm of depth. Using the same Leica microscope, and the same cameras described above, the cells were first recorded in the upright position. Then the petri dish containing the pool was flipped upside down and placed on a different microscope, which was an inverted microscope (Olympus IX71, Japan). The different pictures and videos were recorded using the same CMOS camera with the 10 times objective lens (UPlanFL N, 10×/0.30 Ph1, Japan). Finally, the petri dish was flipped back in the initial position, on the initial Leica microscope, and mineral oil (Nacalai Tesque inc., 23306-84, Japan), biologically inactive, was added on top of the medium containing the cells. In the case of the upside-down condition, the windows size obtained from the camera is 700 μm × 530 μm. Figure 2.3(A) shows these three steps. This procedure was repeated for six different samples, and the extraction of the surface concentration and swimming velocity was extracted as described above. As before, the swimming velocity was obtained from diluted suspension.

The ciliary motions were recorded at 1000 fps using the high speed camera FASTCAM SA3 (Photron, 60KM2, USA) mounted on the phase contrast microscope (OLYMPUS, BXS1WI, Japan) with a 100 times oil objective lens (Olympus, UPlanSApo, Japan). The movie 1 and figure 2.4 were obtained by putting the cells between a microscope slide and a cover slip, hold apart from each other by the double side adhesive tape as shown in figure 2.5 and focusing at the meniscus formed on the side without tape. The movie 2 and figure 2.6 were obtained by using silicon coated microscope slide and cover slip in order to obtain a strait meniscus as shown in figure 2.7. As described before, double side adhesive tape was used to keep the glass slides apart, figure 2.5.

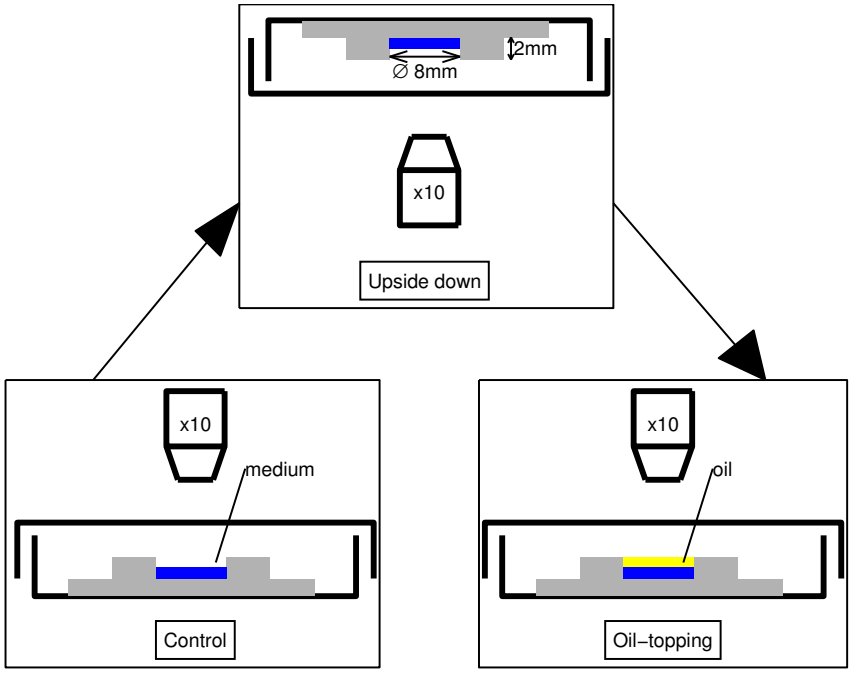

Figure 2.3: Set-up used in order to observe the change of behaviour of the cells when changing the conditions related to taxes.

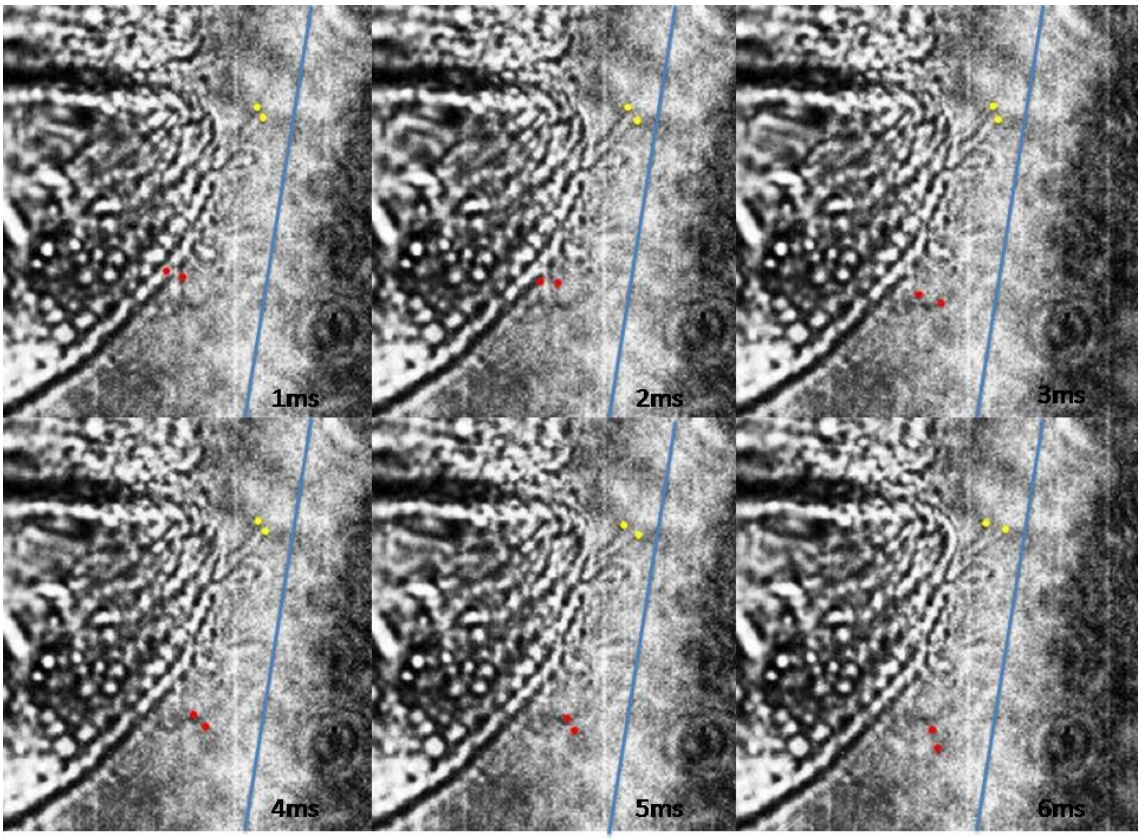

Figure 2.4: At the water-air interface, the ciliary motion of a cell surrounded by numerous cells is stopped. The blue line represents the approximative position of the water-air interface, the air being on the right side.

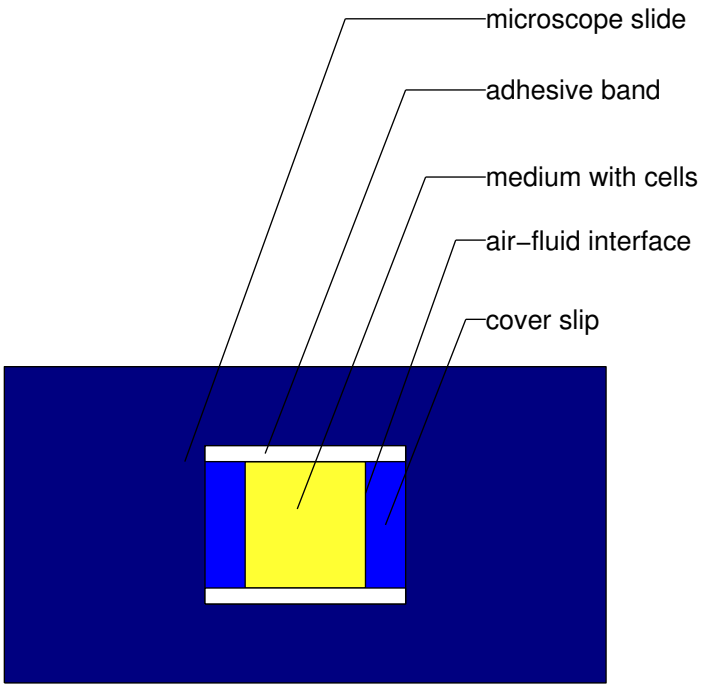

Figure 2.5: Adhesive band of 200 μm thickness is put on two side to allow enough space between the two glass slides for cells to swim freely and have a stable water-air interface. View from the top.

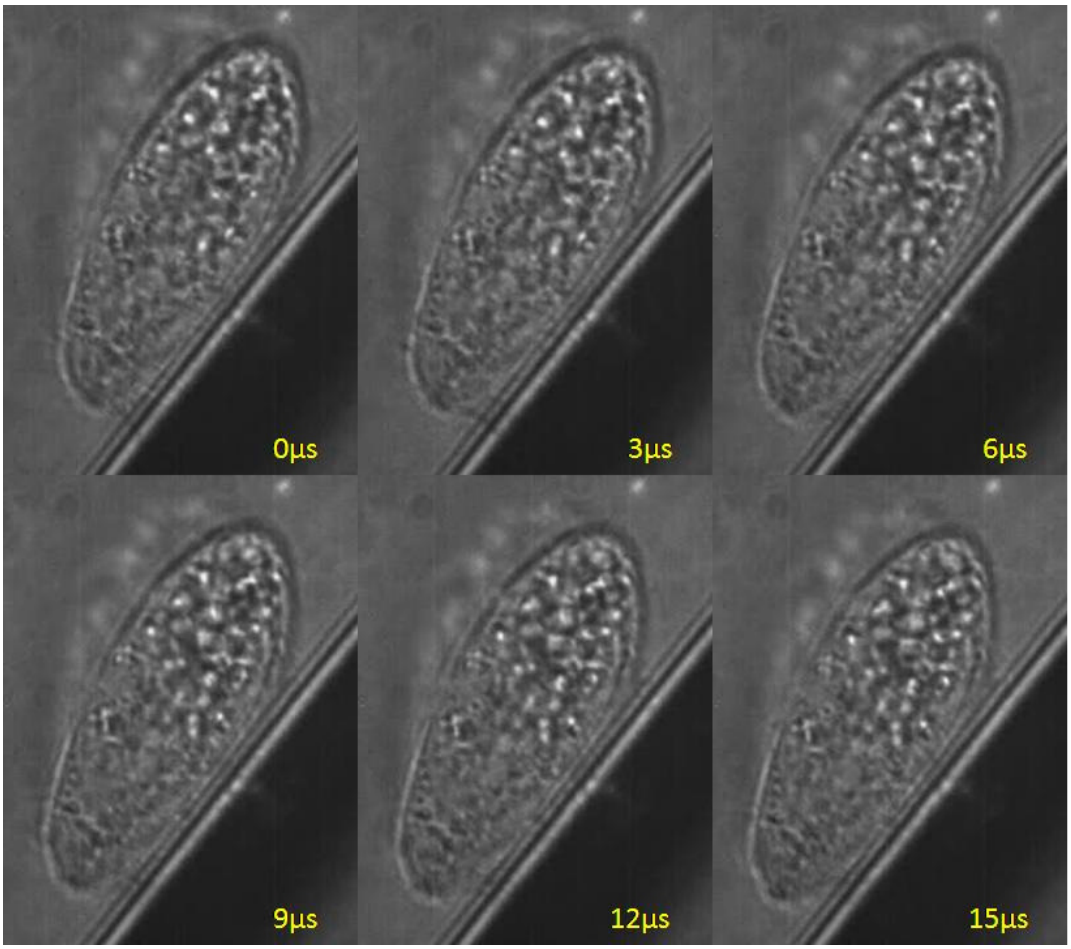

Figure 2.6: *Tetrahymena* is crawling at the flat water-air interface. Supplementary movie 2 is also attached to the thesis.

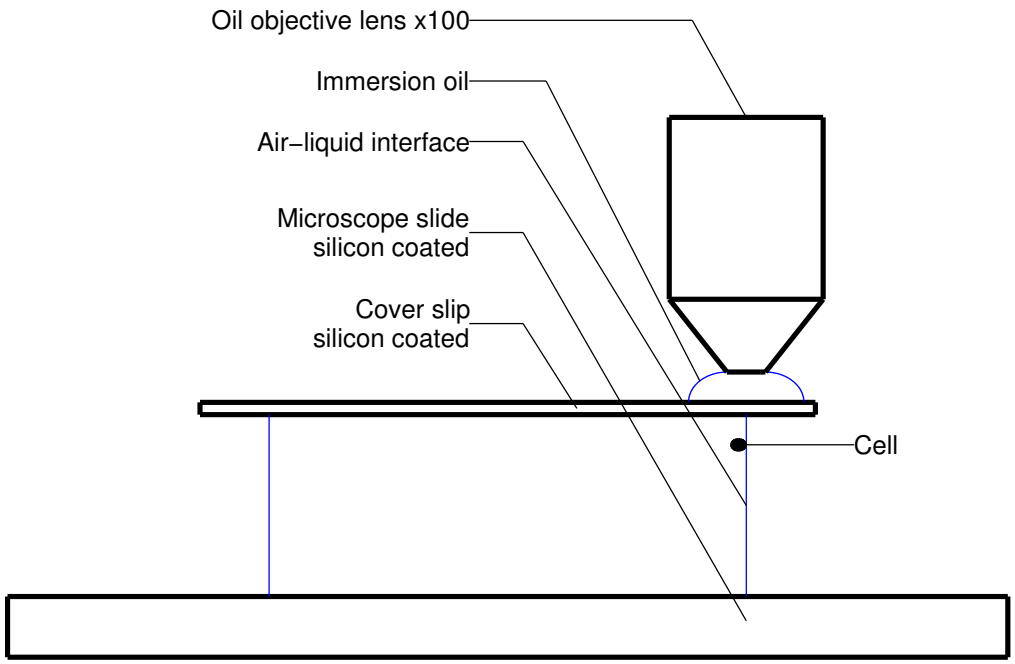

Figure 2.7: Set-up in which the cell was observed crawling.

2.3 Results and discussion

For a starter we had previously observed the entrapment using cells cultivated after a couple of days. We decided then to begin by observing how the behavior of the cells at the water-air interface (WAI) and away from any interface (water-air as well as solid walls) would change during the course of seven days. This observation would give us the day during which the protists would be in their best physiological condition from the shape of the cells and their behavior inside the medium, that is away from any interfaces (AFAI). We characterized the behavior of the cells by using the swimming velocity AFAI and the total concentration of cells. We then compared it to the behavior at the water-air interface also characterized by the swimming velocity at this interface and the surface concentration of cells. The other purpose of detecting the behavior of the cells at the WAI and AFAI simultaneously was to verify if some sort of causality could be established between the cells behavior AFAI and the fact that some cells were trapped at the WAI or at least give us a first hint on the direction to investigate. The plots of the figure 2.8, represent respectively the change of the global concentration of cells during the course of seven days, and the change of the surface concentration of cells during the same period. In figure 2.8(A) we can see the usual growth graph of microorganisms in a medium void from predators. As usual when representing a growth curve, the y-axis is in logarithmic scale while the x-axis is on linear scale. We can observe a first phase of growth from 90 cells.mm^{-3} to 2000 cells.mm^{-3} during the first five days, followed by an almost plateau until the seventh day. On the other hand, the shape of the plot of the change of surface concentration showed in figure 2.8(B) has a sharper first phase, which ends at the third day, but it is also followed by a plateau which is at $\sim$200 cells.mm^{-2} until the seventh. The surface concentration graph is also represented on semi-log y-axis. When comparing the shape of these two graphs, it would seem like, as the concentration inside the medium increases, the surface concentration also increases but reaches a maximum more quickly, maybe because of the limitation of the two-dimensional environment that offers the WAI.

The plots of the figure 2.9, represent respectively the swimming velocity of the cells AFAI and at the WAI. We can see from figure 2.9(A) that the cells swam at approximately the same velocity of 620μm.s^{-1} $\pm$50μm.s^{-1} for seven days. To plot the swimming velocity of the cells at the WAI, we had to work in two different kinds of suspension as shown

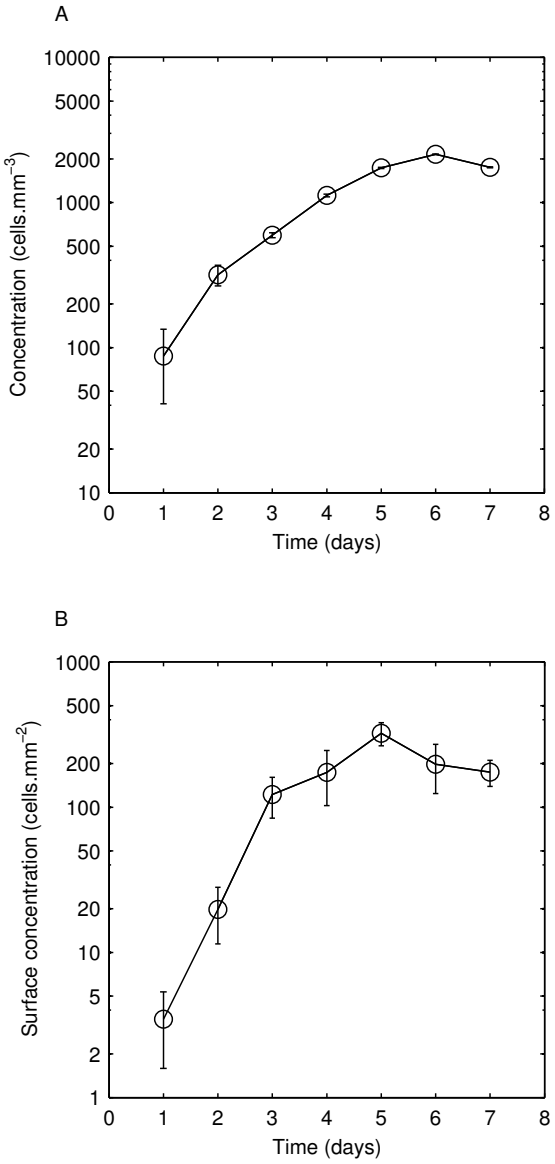

Figure 2.8: Change of the concentrations of cells over the course of seven days. The graphs have a semi-log axis in y. The error bars indicate the standard deviation. (A) Concentration inside the medium. (B) Surface concentration at the water-air interface. The number of cells at the interface is limited due to the two-dimensional geometry, which could explain why the plateau was reached first at the interface.

in figure 2.10. We called natural suspension the suspension we could observe directly after putting it in the PDMS pool from the petri dish where the cells were cultivated, figure 2.10(A). But as we can observe in the figure 2.8(B), the number of cells at the WAI increased with the passing days, and at the same time the velocity of the cells decreased on the fourth and fifth day to $\sim$ 30 μm.s^{-1} as shown in figure 2.9(B). This was partly because the number of cells at the WAI became too large and the swimming was obstructed by the other cells. We then decided to measure the velocity after diluting the medium with cells, figure 2.10(B), in order to avoid cell-cell interactions. In such a case the cells swam as the same velocity of 200μm.s^{-1} $\pm$50μm.s^{-1}. Since inside the medium the three-dimensional swimming prevents more easily to have steric effect, it seemed relevant to compare the swimming velocity AFAI and at the WAI in the diluted suspension. The fact that the cells at the WAI swim at about 1/3 of the velocity at which the cells swim AFAI indicated that the entrapment must be caused by some mechanism, biological or physical, independent from a simple repartition of the cells in the medium. That is, the cells are not simply trapped at the interface because of the high number of cells inside the medium, but because of some other mechanism to be unraveled.

The possibility of the entrapment being the result of surface forces preventing the cells from swimming away easily from the WAI could not be excluded, and needed careful investigate. However, as mentioned in the introduction, *T.thermophila* presents a negative geotaxis and a positive chemotaxis for oxygen. Since the air contains $\sim$21% of oxygen and the cells were observed only when the WAI was above the medium these taxes could explain the entrapment of cells at the interface. Therefore, in addition to the possible physical cause, we had to verify if the entrapment could be related to these taxes. To look into the different possible causes, biological as well as hydrodynamics, we once again looked into their behavior first, and measured their surface concentration and swimming velocity in altered conditions. When looking at the shape of the cells themselves shown in figure 2.11, it is interesting to remark that the fifth day, when the first growth phase of the concentration ends and when the surface concentration seems to have a small peak in the plateau, is the day when the cells appears to have the healthiest shape, that is a pear-like shaped. This encouraged us to choose the fifth day as the day to push further our study of the entrapment and the mechanism behind it. Because of the obvious steric effect highlighted in figure 2.9(B) when working with the natural suspension, it also appeared

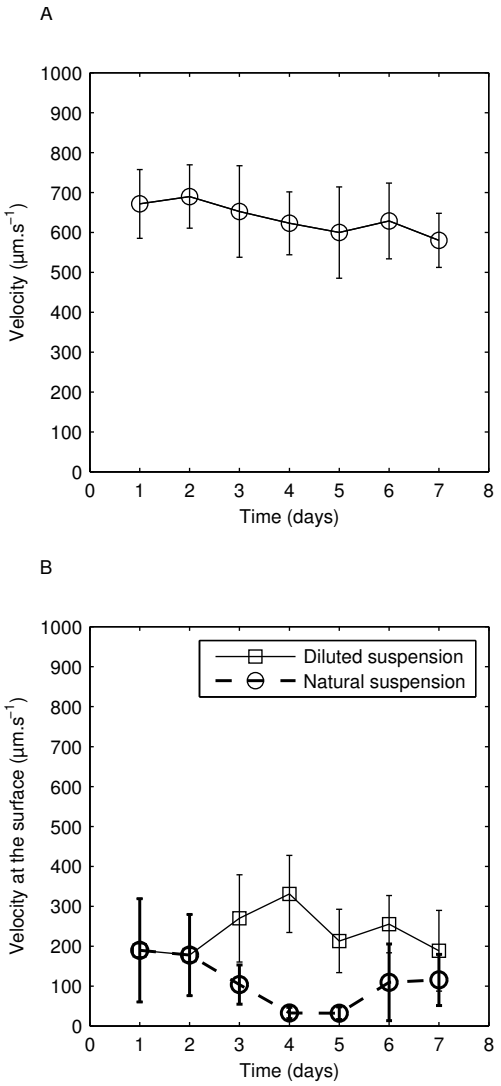

Figure 2.9: Change of swimming velocity of cells over the course of seven days. The axes of the graphs are both linear. (A) Away from any interface, which is inside the medium, the cells swam at $\sim$620 μm.s^{-1} during the seven days. (B) At the water-air interface, both in the natural and diluted suspension the cells swam at 1/3 or less of the velocity at which they swam away from any interface. The difference between the natural and diluted suspension is mostly due to the steric effect when too many cells are trapped at the interface.

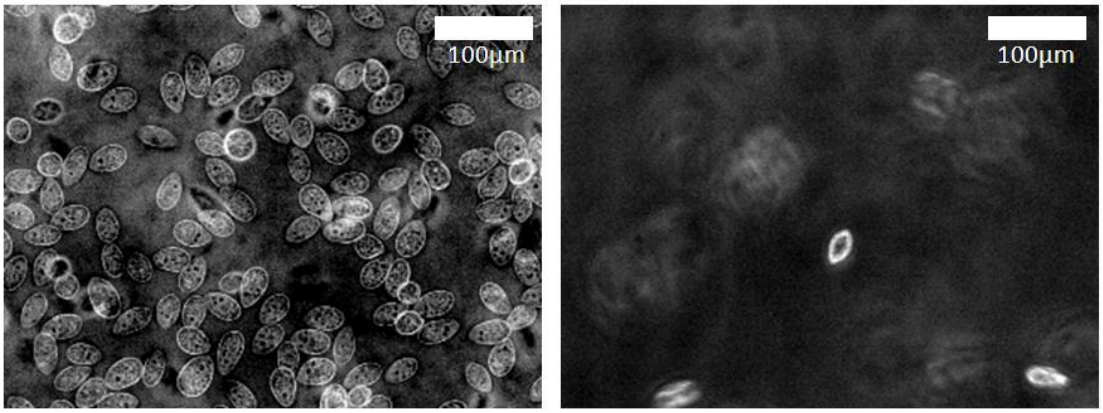

Figure 2.10: Picture of cells at the water-air interface at day 5. (A) In a natural concentration, by simply pouring the cells in the PDMS pool directly from the petri dish in which they were cultivated. (B) In a diluted suspension, that, the medium containing cells is diluted before being poured in the PDMS pool. In this case the cell-cell interactions become a rare occurrence.

necessary to work with a diluted suspension when considering the velocity. We decided to begin by looking into the physiological possible influences.

To evaluate the effect of the taxes on the entrapment, we created two different conditions in order to separately deprive the cells from the influence of these taxes. Each sample was then submitted to three successive observations. First, the cells were observed in the control condition, that is they were poured in a 8 mm of diameter PDMS pool enclosed in a petri dish and observed using an upright microscope. In a second time, the diameter of the pool being small enough to prevent the liquid from falling, the petri dish containing the pool was turned upside down and observed using an inverted microscope. During this step, the medium was above the WAI, therefore the negative geotaxis lead the cells to swim away from the WAI. And finally the petri dish was flipped back in the upright position, and mineral oil was added on top of it. During this final step the WAI became an oil-water interface, keeping therefore the physical properties of a stress free interface, but suppressing oxygen from the non aqueous phase above the medium. If cells were aggregating at the WAI because of the oxygen, they should not aggregate at the oil-water interface since the oil used is biologically inactive. In figure 2.12(A), and figure

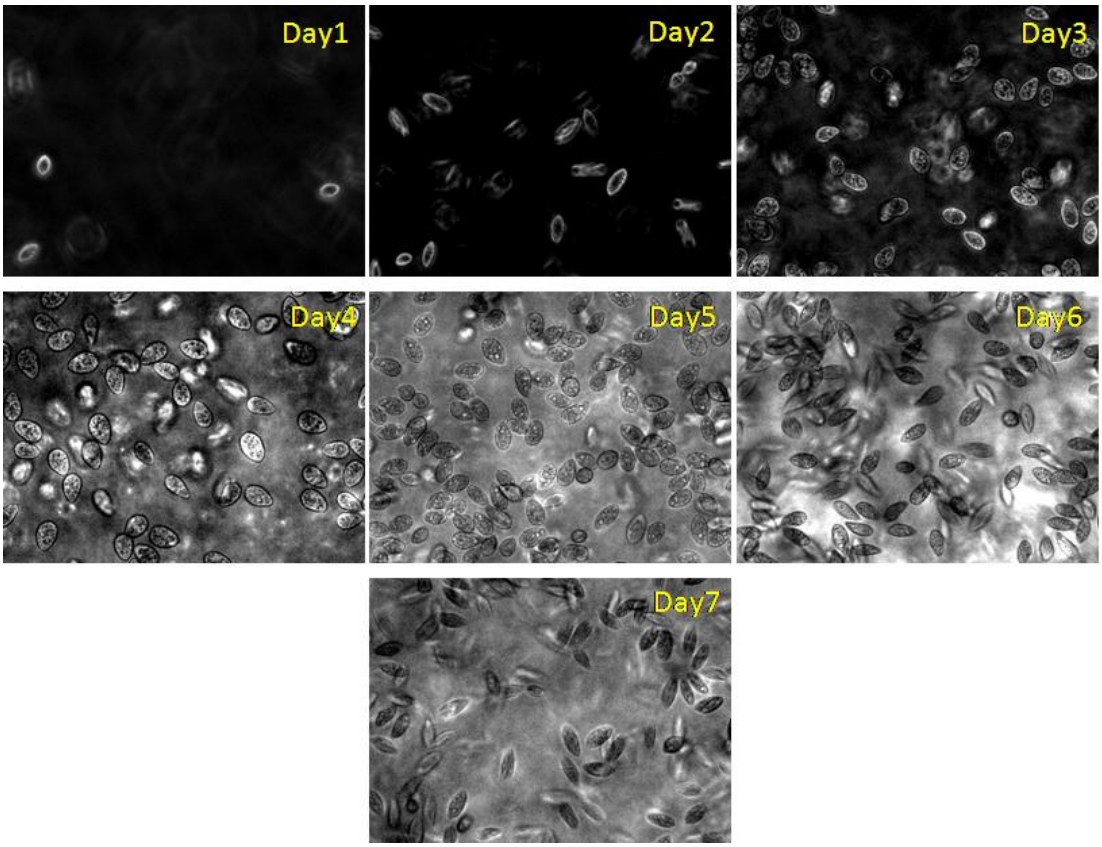

Figure 2.11: Picture of the cells trapped at the water-air interface at different days after inoculum from day 1 to day 7.

2.13, we can see that the concentration of the number of cells trapped at the WAI doesn't decrease. In addition, figure 2.12(B) reveals that the velocity of the cells at the free WAI is not greatly modified in the three conditions, but was still significantly lower, in the range 100-200μm.s^{-1}, than the swimming speed AFAI, $\sim$600μm.s^{-1}. The two taxes therefore seem to have little influence on the entrapment of the cells at the WAI. Therefore we moved on towards the possibility of the entrapment being the effect of the surface tension.

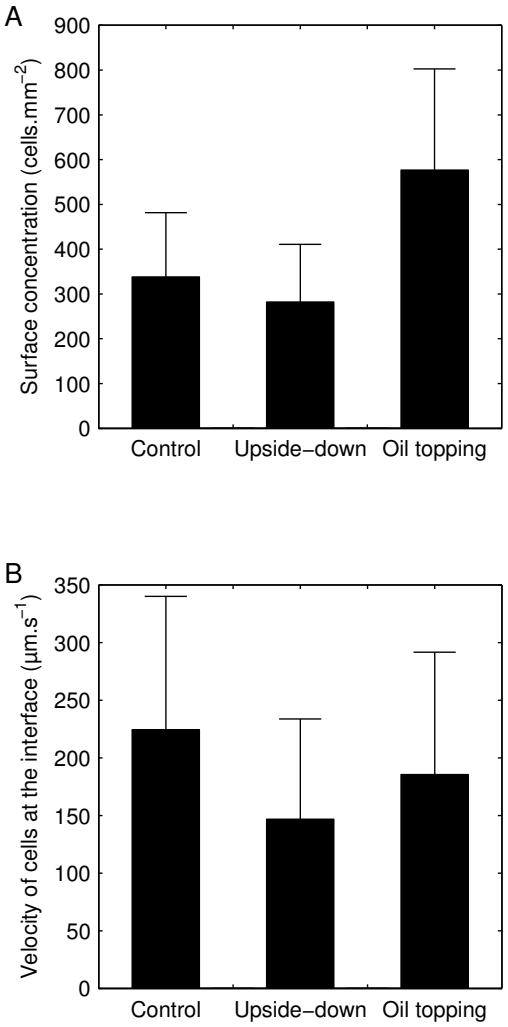

Figure 2.12: Observation of cells in three different conditions in order to verify the effect of geotaxis and chemotaxis on the entrapment. Control: 120 μl of medium with cells are first put in the pool. Upside-down: the pool is then turned upside-down in order to verify the effect of geotaxis on the entrapment at the WAI. Oil topping: the pool is then turned back in the upright position and mineral oil is poured on the top of the medium containing the cells to verify the effect of chemotaxis for oxygen on the entrapment. (A) Surface concentration. (B) Velocity of cells at the WAI.

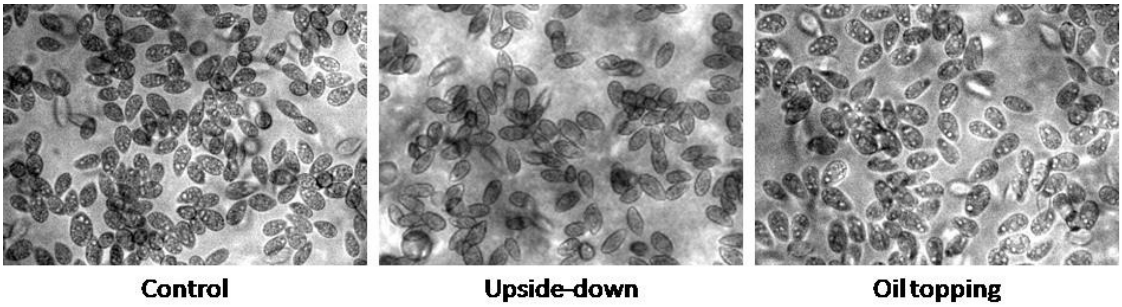

Figure 2.13: Cells trapped at the interface respectively in the control condition, the upside-down condition and the oil topping condition described in figure 2.12

Seeing how the number of cells changes in figure 2.8(B), we wanted to see if the presence of cells would affect the surface tension during the seven days of culture. As we can see in figure 2.14, the surface tension increases from $\sim$53mN.m^{-1} to $\sim$67mN.m^{-1} during the first five days. It then decreases to $\sim$64mN.m^{-1} during the following two days. Even though the curve somehow follows the one of the number of cells at the WAI during seven days, we couldn't tell clearly if the change of surface tension was causing the entrapment or if the entrapment was causing the change of surface tension. In order to clarify the possible causality between the change of surface tension and the change of number of cells at the WAI, a new experiment was devised in which, by adding small amount of surfactant, we could lower the surface tension and see how this affected the number of cells trapped. Using the surfactant Tween20, we obtained the figure 2.15(A) and 2.15(B). The number of cells suddenly drops to zero when the surface tension becomes lower than $\sim$42mN.m^{-1}, while it is constant when above this value. We can observe an increase of swimming velocity from $\sim$200μm.s^{-1} to $\sim$450μm.s^{-1} when the surface tension becomes lower than $\sim$44mN.m^{-1}. However the surface concentration of cells does not change much when the surface tension is larger than $\sim$42mN.m^{-1}. This result corresponds well to the fact that the entrapment phenomenon was not affected by the surface tension in the natural culture fluid. We note that the threshold value changes with the kind of surfactant. Such results would have confirmed the role of the surface tension in the entrapment if not for the other effect of surfactants. Not only does surfactant change the surface tension but they also

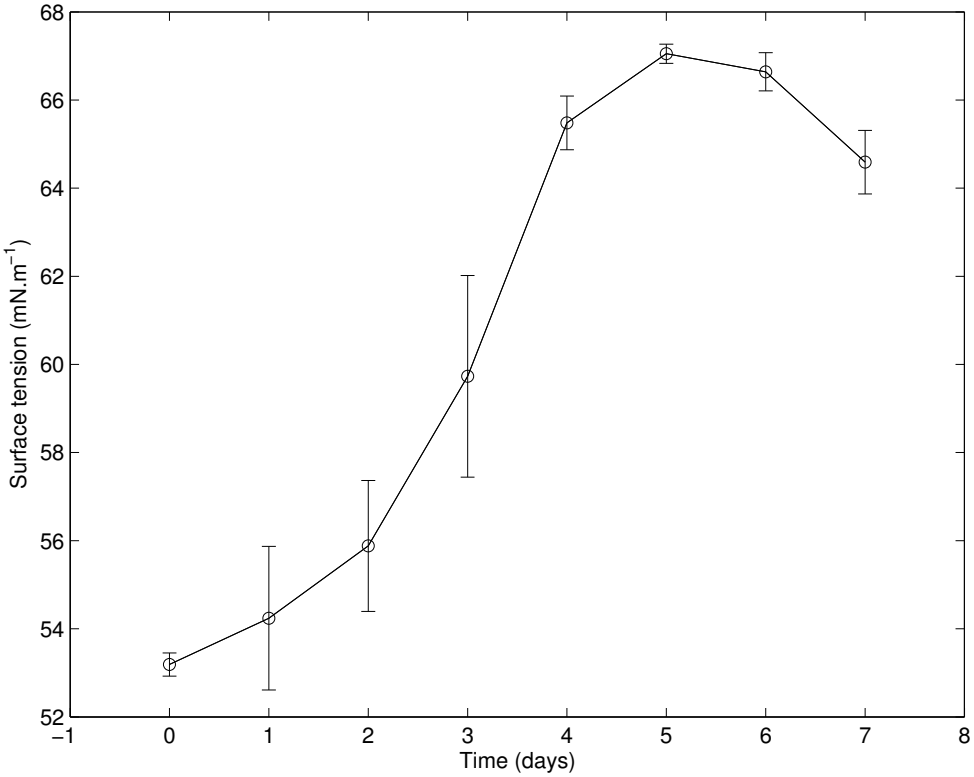

Figure 2.14: Change of the surface tension of the culture fluid during the seven days after inoculum.

modify the mobility of fluid particles at the WAI in the plan of the WAI by inducing effects such as the Marangoni effect. In the Marangoni effect, when heterogeneity in the surfactant concentration appears at the interface, a back flow is generated in order to homogenize the repartition of surfactant at the interface. Therefore the WAI has the same "rigidity" as a solid wall where cells are not trapped. It is remarkable to see how this last possible interpretation seems to be supported by the work of Nicola Ricci [20]. He reported how Oxytricha bifaria is creeping at the velocity of 220 μm.$^{-1}$ at the WAI while creeping at 550 μm.$^{-1}$ on solid substrates, which is quite similar to how *Tetrahymena* crawls at $\sim$200μm.s^{-1} when little surfactant is present at the WAI but accelerate to $\sim$450μm.s^{-1} in presence of enough surfactant.

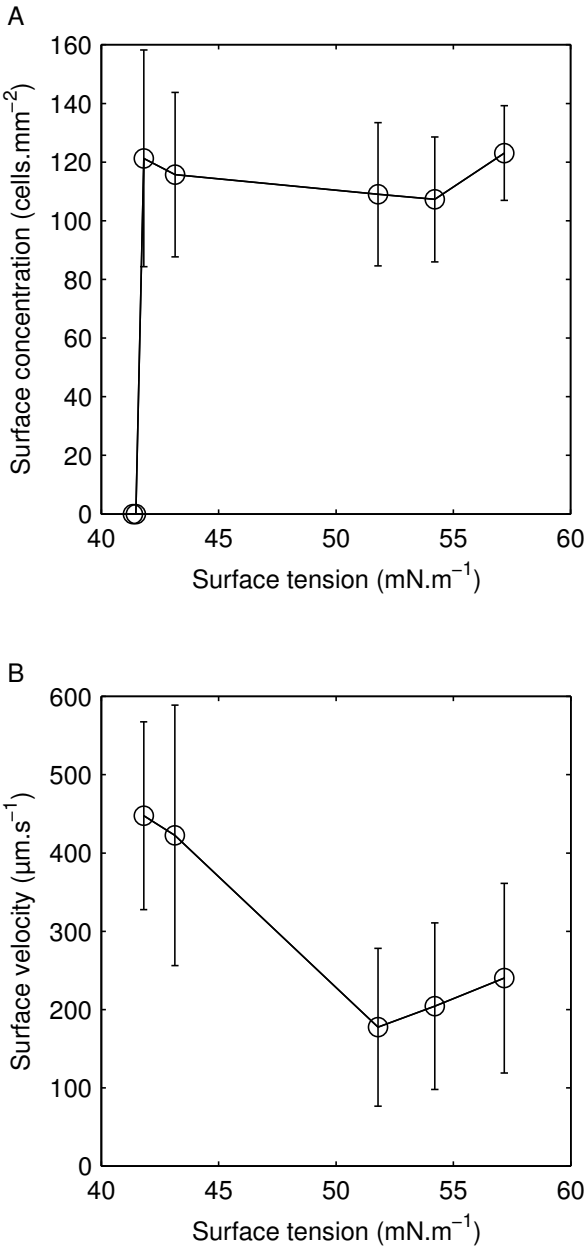

Figure 2.15: The surface tension of the culture fluid at day 5 after inoculum was lowered by adding the surfactant Tween 20 in order to see the effect on the entrapment. (A) Surface concentration of cells. (B) Swimming velocity of the cells at the water-air interface.

Since the cells apparently interacted with the WAI because of some interfacial properties, and since the velocity of the cells greatly decreased at the WAI, we decided to see how the cilia moved when close to the interface. We basically succeeded to observe the ciliary motion in two different set-ups giving possibly opposite interpretations. In figure 2.4 and movie 1 we can observe how the cilia close to the WAI are stopped. To observe this ciliary motion, we put the cells between a microscope slide and a cover slip, and focused on the cell as indicated in figure 2.16. We can see on the movie 1, the cilia on the top of the cell, the closest to the cover slip are still beating while the ones on the side, close to the interface (in the zone of transition in the light intensity) are stopped. On the other hand, in figure 2.6 and in movie 2, we can observe the cell crawling at the WAI. For this set-up, we have used a cover slip and a microscope slide coated with silicon in order to have a flat interface normal to the microscope slide. We observed the cell from the top as shown in figure 2.7. When watching this movie, it is easier to see the crawling motion of the cells as well as the fact that cilia move at the WAI, transition zone indicated in one of the picture of figure 2.6. When seeing movie 1, we could conclude that the cilia are trapped by the WAI, but when watching the movie 2, it would appear like the cilia can move freely. In the movie 1, the cell is surrounded by number of other cells and cannot swim sideways or backward. Taking this into account it would not be surprising to find that the motion of the cilia were stopped because of the rigidity of the cilia. The cilia would then be stopped by the interface and the impossibility of the cell to move because of its neighbors, and not because of the interface trapping the cilia by interfacial forces.

In this chapter we have ascertained that the entrapment of the cells at the WAI could be explain by interfacial physics. In the following chapter we use mathematical tool to clarify the mechanism behind this phenomenon.

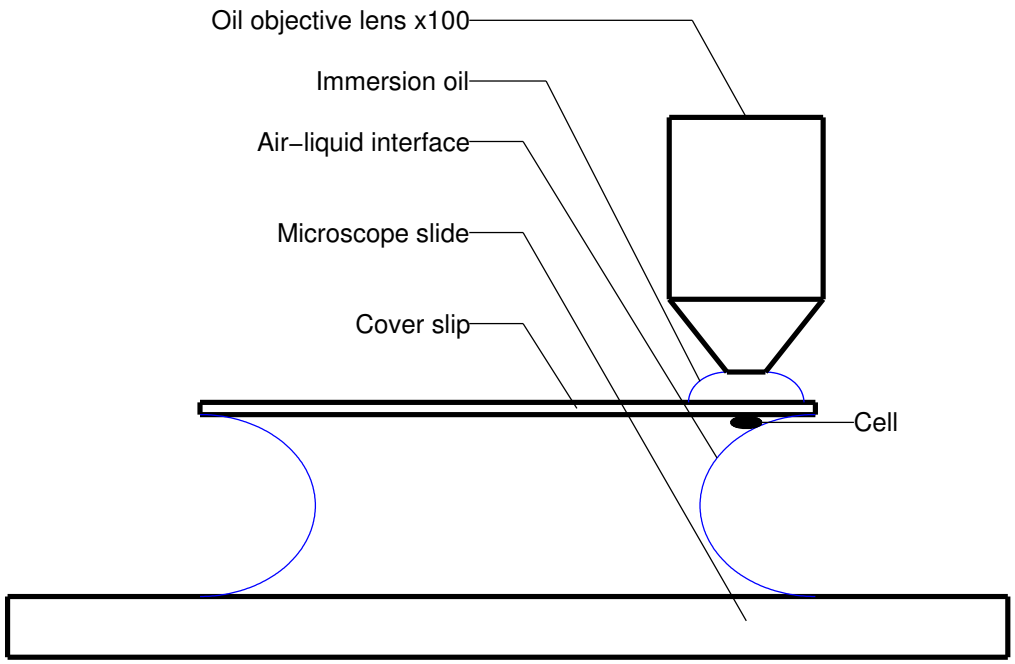

Figure 2.16: Set-up in which ciliary motion was observed stopped.

2.4 Summary

In this chapter, we have reported the existence of a novel phenomenon: the entrapment of ciliated microorganism at the water-air interface. We characterized it, and observed that when the cells are trapped at the interface they swam at 1/3 of the velocity at which they swam inside the medium. We have clarified that the mechanism behind this entrapment can be explained but by surface physics.

Chapter 3

Numerical analysis: Entrapment of model ciliate

3.1 Introduction

The modeling of ciliated microorganisms has become a widespread exercise in research, allowing to explain things such as dancing *Volvox* [5] or the biovection pattern of gyrotactic cells [35]. So have been the study of cell-cell interactions in a fluid [36] and the behavior of a swimmer close to solid surfaces [4, 27]. However, not being aware of the entrapment of cells at the air-fluid interface, no modeling of entrapment phenomenon has been performed yet. In chapter 2 we certified the existence of the entrapment of the ciliated cells *Tetrahymena thermophila* at the WAI. But while we tried to explain the mechanism behind it, we began to consider the possibility that the mobility of fluid particles at the WAI could possibly affect the entrapment. In addition, even though we observed entrapment at the WAI, we didn't observe any entrapment of the cells close to a solid wall. We therefore decided to use numerical modeling of a ciliated microorganism swimming close to stress-free surface and a solid wall, to shed light on the possible hydrodynamics causing such behaviors at the interfaces.

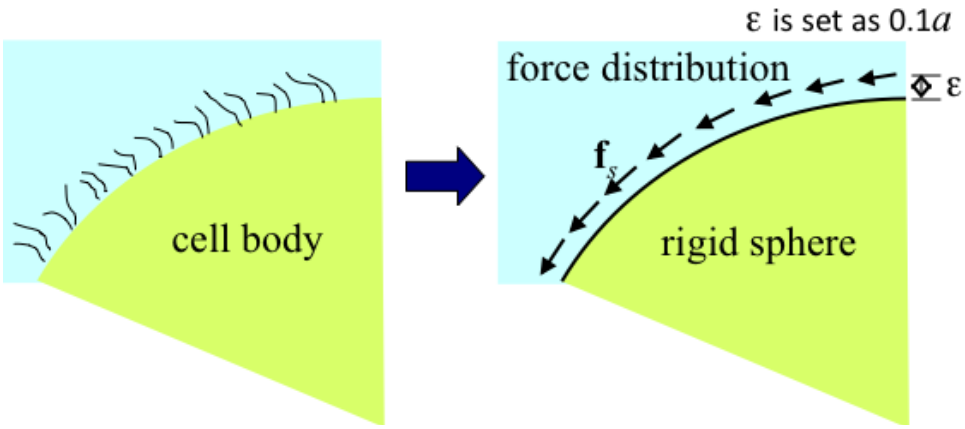

Figure 3.1: Cell body and cilia motion are represented as a rigid sphere with a force shell outside the sphere.

3.2 Methods

Because we need to calculate the flow and stress field, at the interface, the cell surface and inside the layer of beating cilia, the following boundary conditions must be satisfied: the stress-free condition at the WAI, and the no-slip condition at the solid wall and the cell surface. Not sure of how the flow field would change close the stress free interface, instead of working with a fixed flow field around the cell, the force condition in the layer of beating cilia was expressed as a shell of force density. In this study, *Tetrahymena* is thus modeled as a rigid sphere to represent the cell body. A spherical shell having a force density slightly outside that of the rigid sphere represents the layer of beating cilia, fig. 3.1. The cell is assumed to be force-free and torque-free, and the force density distribution is invariant with respect to time. A Stokesian flow field (i.e., no inertial effect) is assumed around the cell. The motions of the model cell in the vicinity of the interfaces are solved numerically by boundary element method.

We first measured the velocity field around a free-swimming *Tetrahymena*, using a confocal micro-PIV system [40] with fluorescent beads of 1 μm. The cell's swimming was recorded at 500 fps using the high speed camera FASTCAM SA3 (Photron, 60KM2,

USA) mounted on the confocal microscope (OLYMPUS, BXS1WI, Japan) used with a 100 times oil objective lens (Olympus, UPlanSApo, Japan) as shown in figure 3.2. The system allowed us to measure the velocity field with very high precision in time and space. The analysis was performed using the software K2 (Seika corporation, Japan), the pattern recognition was perform with multi-pass interrogation algorithm on a 32 $\times$ 32 pixels window for a 50% overlapping. As we extracted the flow field around the cell while it was moving in the fluid, the trajectory of the cell was then manually extracted, from the same movie used for the micro-PIV analysis, using the plugin MtrackJ on the software ImageJ (http://rsbweb.nuh.gov). The velocity of the cells was then finally removed from the flow field obtained with K2. The measured velocity field was then interpolated to calculate velocity at the surface of *Tetrahymena*, in the same manner with Ishikawa & Hota (2006) [36]. This was repeated for three different cells picked in order for them to have the same body scales. The results showed that the surface tangential velocity of *Tetrahymena* was distributed almost sinusoidally from the anterior end to the posterior end figure 3.3(A). *Tetrahymena* was found to be more of a neutral swimmer, similar to *Volvox* [41], as compared with *Paramecium* that was a puller as reported by Ishikawa & Hota (2006) [36].

In order to simplify the modeling of the cell, the squirmer was created as a rigid sphere of radius a. We imposed on this sphere two sorts of force-velocity conditions. First, no-slip boundary condition on the cell body, and then a force density distribution $\boldsymbol{f}_s$ generated by ciliary beat, just above the cell body. The cilia length of *Tetrahymena* being $\sim 5\mu$m [37], that is $0.1a$ of the cell radius body, the force density shell was generated on a spherical surface $0.1a$ above the squirmer body. In a spherical coordinate system, $\boldsymbol{f}_s$ can be split into three components as $\boldsymbol{f}_s = (f_r, f_\theta, f_\phi)$, where r is the radial direction, θ is the polar angle measured from the orientation vector, and ϕ is the azimuthal angle. We assumed that f_θ was constant on the entire spherical shell; because the surface velocity measured experimentally was almost sinusoidal, figure 3.3(A). The radial and azimuthal components were neglected, i.e. $f_r = f_\phi = 0$, given that the ciliary beat mainly generated a thrust force in the θ direction. We numerically confirmed that the velocity field generated by the force density shell of the present model matched well with the experimental results, before performing the actual calculations as shown in figure 3.3(B).

The flow field around *Tetrahymena* was assumed to be Stokesian, because the Reynolds

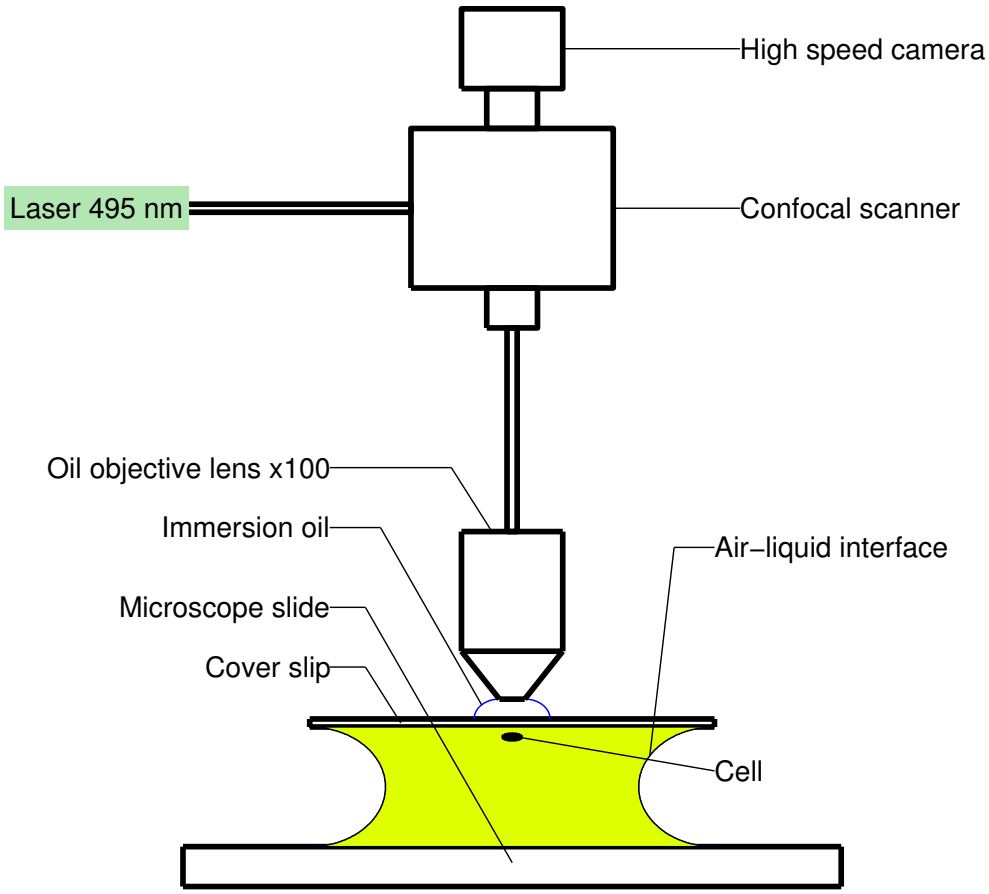

Figure 3.2: The laser illuminated the green-yellow beads in the medium. The swimming of the cells was recorded ~ 50 μm from the cover slip.

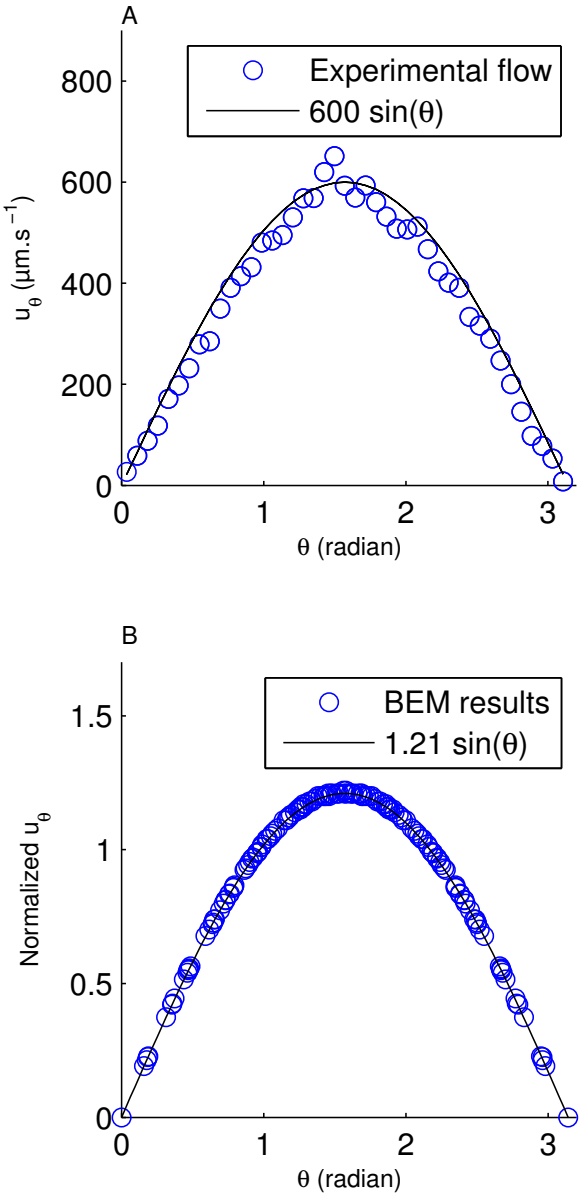

Figure 3.3: Repartition on the flow field around the cell. Angle 0 being the front of the cell and π being the bottom. The flow is assumed axisymmetric. (A) Flow field calculated from experimental data with the fitting curve. (B) u_θ component of the velocity generated on the force density shell of the squirmer model. The flow field has been normalized by the swimming velocity of the cell.

number for swimming *Tetrahymena* was much less than unity, that is $\simeq 10^{-5}$. The effects of sedimentation and bottom-heaviness were neglected, i.e., the model was force-free and torque-free, equation 3.1.

$$\mathbf{F} = \int \mathbf{f} dA_c = 0 \quad \mathbf{T} = \int \mathbf{f} \wedge \mathbf{r} dA_c = 0 \tag{3.1}$$

with $\mathbf{f}$ the force field and A_c the surface on the force shell.

In case of the solid wall, we considered that the model cell exists in a fluid under an infinite flat interface satisfying the no-slip boundary condition. For the WAI, we imposed stress-free boundary condition, and assumed the interface is flat. As we are at low Reynolds number, that is low velocity at small length scale, the thrust force of the cells is defined by $F = 6\pi\mu U a \frac{4+\frac{a}{b}}{5}$ [38]. This equation links the swimming velocity of the cell $U = 600\mu\text{m}.^{-1}$ to the force necessary to go at such a velocity in a fluid of viscosity $\mu = 1000$ when considering an oblong object with a long axis of $2a = 50\mu$m and a small axis of $2b = 20\mu$m swimming in the direction of the long axis. This gives then $F \simeq 3.4 \times 10^{-10}$ N. Therefore, the difference of pressure that could be induced by a cell swimming straight up toward the interface would be $\Delta P = \frac{F}{\pi a^2} \simeq 0.1$ Pa, and the radius of the deformation at the interface induced by the cell becomes $R = \frac{\gamma}{2P} \simeq 0.2$ m, with $\gamma = 64$ mN.m^{-1} as obtained in chapter 2. That is about the deformation would have a radius 10000 times bigger than the radius of the cell and we can therefore consider the interface as flat.

The governing equation for the velocity field $\boldsymbol{u}(\boldsymbol{x})$ is given by:

$$\boldsymbol{u}(\boldsymbol{x}) = \int \mathbf{J}(\boldsymbol{x} - \boldsymbol{y}).\boldsymbol{q}(\boldsymbol{y}) dA_c + \int \mathbf{J}(\boldsymbol{x} - \boldsymbol{y}).\boldsymbol{f}_s(\boldsymbol{y}) dA_f \tag{3.2}$$

where $\boldsymbol{q}$ is the traction force, A_c is the surface of cell body, A_f is the surface of force-density shell, and $\mathbf{J}$ is the Green function. The half-space Green functions for the stress-free interface and the no-slip interface were derived by Blake (1971, 1978) [28, 29] as introduced in the introduction section and reminded in the equations 3.3 and 3.4. On the surface A_c the traction force is unknown, whereas on A_f the velocity is unknown. Equation(3.2) is solved by the boundary element method, which couples with the force-torque conditions of the cell bodies. We also introduced a short-range repulsive force, similar to [36], to avoid overlapping the force density shell and the interface and prohibitively small time step, when two surfaces come very close. The trajectories were calculated by the fourth order Adams-Bashforth time-marching method. The details of these numerical methods

can be found in Ishikawa et al. (2006) [36]. When close to an interface (stress-free as well as no-slip conditions), no modification of the force field ($\mathbf{f}_s = constant$) was introduced since we assumed no change of the ciliary motion close to the interface. This assumption came from the observation in movie 4 that the beads can flow above the cells and in movie 2 that there is no apparent disturbance of the ciliary motion. The force field was then considered independent of position of the cell and in time. The boundary conditions and simplifications detailed above are shown in figure 3.4.

$$J_{ij} = \frac{1}{8\pi\mu}\left[\left(\frac{\delta_{ij}}{r}+\frac{r_i r_j}{r^3}\right)-\left(\frac{\delta_{ij}}{R}+\frac{R_i R_j}{R^3}\right)+2h(\delta_{j\alpha}\delta_{\alpha k}-\delta_{j3}\delta_{3k})\frac{\partial}{\partial R_k}\left(\frac{hR_i}{R^3}-\frac{\delta_{i3}}{R}-\frac{R_i R_3}{R^3}\right)\right] \tag{3.3}$$

$$J_{ij} = \frac{1}{8\pi\mu}\left[\left(\frac{\delta_{ij}}{r}+\frac{r_i r_j}{r^3}\right)+(\delta_{j\alpha}\delta_{\alpha k}-\delta_{j3}\delta_{3k})\left(\frac{\delta_{ij}}{R}+\frac{R_i R_j}{R^3}\right)\right] \tag{3.4}$$

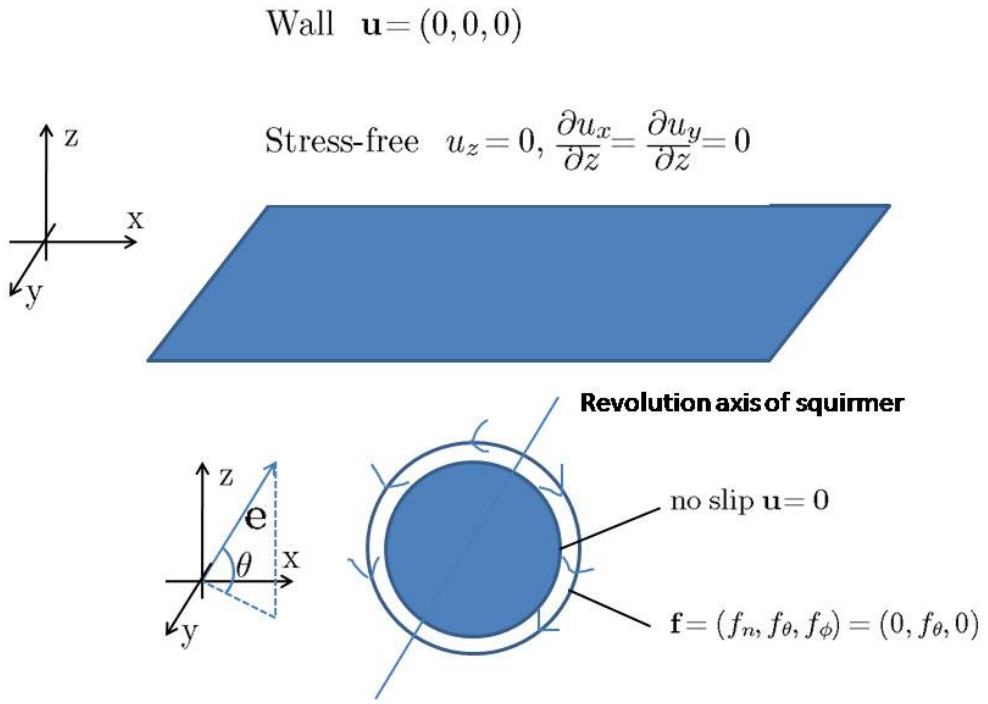

Figure 3.4: Boundary conditions applied to the squirmer when it's close to an solid wall and a stress free interface.

3.3 Results and discussion

We first computed the trajectory of the model cell in the vicinity of a no-slip and stress-free surface respectively. The model cell is initially placed at $(x, y, z) = (0, 0, -2)$, where surface is placed at $z = 0$ and x and y axes are parallel to the surface. The length scale is non-dimensionalized by the radius of the sphere and the time scale is non-dimensionalized by using the radius and the swimming speed of the cell AFAI. The orientation vector of the cell is initially placed in the $x - z$ plane and remains in the same plane during swimming, due to the symmetry of the problem. The initial angle θ is defined as the angle between the initial orientation vector and the x-axis, i.e. $\theta = 0$ indicates a direction parallel to the surface, whereas $\theta = 90$ deg indicates the direction perpendicular to the surface (surface normal), as shown in figure 3.4. Figure 3.5(A) shows the trajectory of the model cell near the no-slip surface, with various initial orientation angles. The cell's center cannot come closer than $z < 1.1$, due to the short-range repulsive force between the no-slip surface and the force density shell with a radius of 1.1. The circles in the figure are plotted with the same time interval of 0.4 time unit; thus, the velocity of the cell in the x (or z) direction is proportional to the distance between two successive circles in the x (z) direction. The decrease in the swimming velocity near the no-slip surface was not significant in all cases. For angles of approach of $\theta = 15$ deg the cells don't even get close to the no-slip surface, and for the other angles they come close to it for a short time before swimming away. In the case of stress-free surface, figure 3.5(B), the cell with $\theta = 15$ deg come close to the interface even though it doesn't when it is a no-slip surface. By comparing cells with $\theta = 30$ or 45 deg between the stress-free and the no-slip surface cases, it was found that the cell tend to stay longer near the free surface than near the no-slip surface. In the case of $\theta = 60$ deg, the cell is actually trapped at the stress-free surface.

These results are consistent with experimental observations. The cells are not trapped near the solid wall, but instead, swam away from the wall without a significant decrease in their velocity while they stayed a significant longer time at the WAI and greatly decreased their velocity when there.

We then computed the orientation of the cells in regard of the interfaces when swimming close to the interfaces. Figure 3.6(A)(B) shows the z-component of the orientation vector, where $e_z = 1$ indicates the orientation perpendicular to the surface, whereas $e_z = 0$

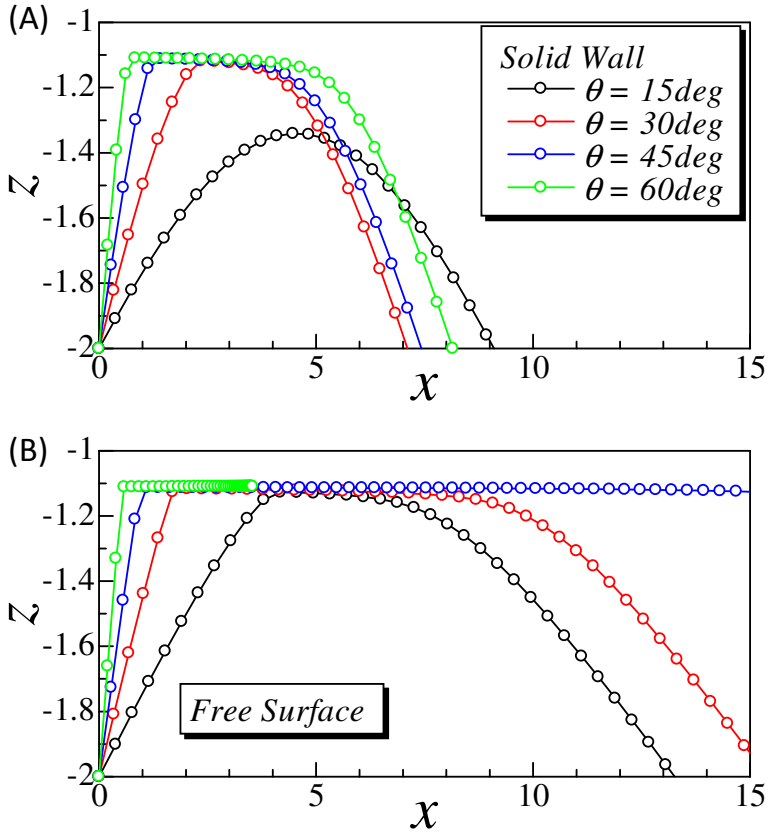

Figure 3.5: Trajectory of a squirmer swimming close to two different types of interface, where the interfaces exist at z=0. x/a is the normalized coordinate parallel to the interfaces for different initial angles of approach. a is the radius of the squirmer. The time interval between successive circular points is $0.4a$/U, where U is the swimming speed. (A) When the interface is a water-solid interface. (B) When the interface is an water-air interface.

indicates a direction parallel to the surface. In case of the no-slip surface, for the different initial angles of approach, the cells gradually change their orientation until they are swimming away from the no-slip surface as we can observe when comparing with figure 3.5(A). In the vicinity of the stress-free surface, figure 3.6(B), when compared in the case with the no-slip surface, the cells need a significant higher amount of time to orient themselves away from the stress-free surface and the reorientation is far less efficient than in the no-slip surface case as we can see when comparing both final orientations. This result clearly illustrated that the rotational velocity needed to redirect the cell away from the surface was considerably suppressed by the stress-free condition at the interface. This was mainly because the rotational velocity of the cell was reduced in the stress-free surface case. Exception was the angle of $\theta = 60$ deg, the cells are oriented toward stress-free interface, and eventually swam vertically upwards which explain the trajectory of figure 3.5(B).

When comparing the behavior of the cells close to the two interfaces, and taking into account that the stress-free interface was considered flat, this suggests that the stress-free condition at the WAI is one of the main mechanisms of the entrapment phenomenon found in the experiments described in chapter 2. That is the ability of the fluid to move freely at the interface in the plan parallel to the WAI prevents the cells from swimming easily away from it. The results obtained by the numerical approach could have been somehow foreseen using leading order term of the lubrication theory of a sphere moving very close to an interface which equations are mentioned in the introduction chapter, and detailed in Ishikawa et. al. (2006) [36].

In the present cell model, the surface velocity is generated on the force density shell, which has mainly the tangential velocity component, due to the no-slip boundary condition on the cell body. A squirmer is thus a good simplified model to understand the hydrodynamics of the model cell near the interface. The results of Ishikawa et. al. (2006) [36] showed that the torque exerted by the squirmer is proportional to the velocity difference δu between the interface and the squirmer surface. The leading order term in the lubrication theory is $\delta u \log(1/\varepsilon)$, where ε is the gap between the two nearby surfaces. To simplify the discussion, let the squirmer be placed parallel to the interface without translational and rotational velocities. When the interface satisfies the no-slip condition, like a solid wall, the velocity on the squimmer surface is u_s, where u_s is the squirming velocity in the lubri-

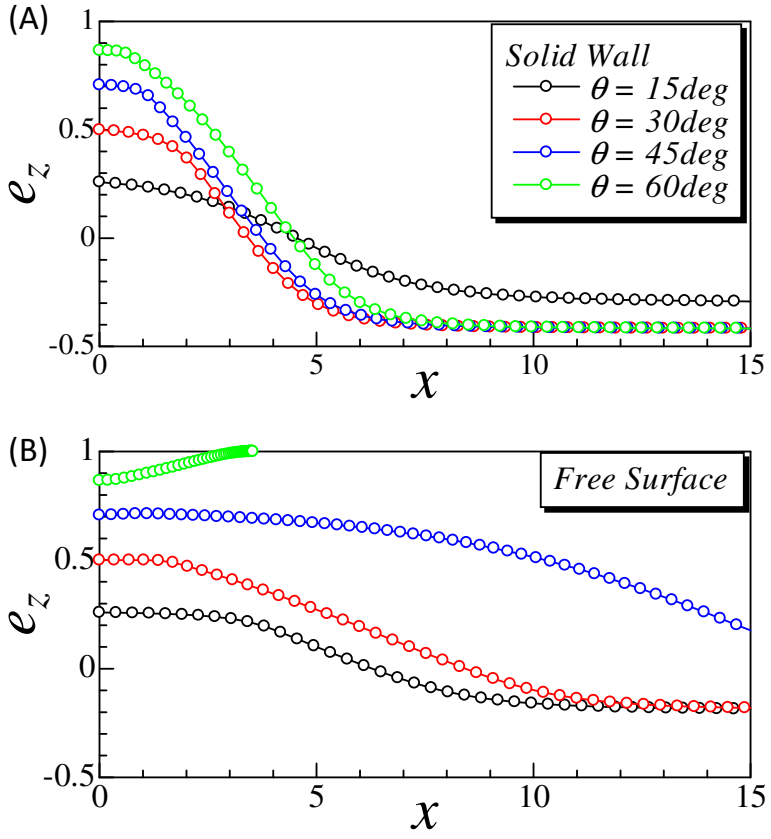

Figure 3.6: Change in the z-component of the orientation vector of a squirmer swimming close to two different types of interface, where the interfaces exist at z=0. x/a is the normalized coordinate parallel to the interfaces for different initial angles of approach. a is the radius of the squirmer. The time interval between successive circular points is $0.4a$/U, where U is the swimming speed. (A) When the interface is a water-solid wall interface. (B) When the interface is an air-liquid interface.

cation region, and the velocity on the solid wall is 0. Thus $\delta u = u_s$ and the leading order term of the exerted torque is proportional to $u_s \log(1/\varepsilon)$. The squirmer tends to orient away from the solid wall, due to the torque. In this case, the rotational velocity is again proportional to $u_s \log(1/\varepsilon)$. This is the main mechanism attributed to why the model cell swims away from the solid wall. When the interface satisfies the stress-free condition, on the other hand, the tangential component of the velocity at the interface has no gradient in the normal direction. Thus, the velocity becomes u_s both at the squirmer surface and at the stress-free interface, i.e. $\delta u = 0$, and the leading order term in the lubrication theory disappears. Because the next order effect comes not only from the lubrication region, but also from the whole cell body, the hydrodynamics in this case becomes qualitatively different from that with the no-slip surface and a weaker torque is applied on the squirmer. This is the main reason for why the model cell behaves differently at the no-slip and the stress-free interfaces. From these results, we can say that the entrapment can be explain by stress-free boundary condition.

3.4 Summary

In this chapter, we clarified the mechanism of the entrapment. We modeled the cell as a squirmer with the following conditions: constant force shell around the squirmer because we neglected the possibility of cilia motion being disturbed by the air-fluid interface as suggested by videos 2 and 4; no-slip boundary condition of the squirmer body. The motion of the squirmer was considered when close to a solid wall and close to a water-air interface. The solid wall was represented by a flat surface with no-slip condition on it. Since, from our scaling and the movie 2, the cells were unlikely to deform the water-air interface, the interface was modeled as a flat surface. Stress-free condition was applied on it. The numerical simulation leads to qualitatively similar behaviors of cells as in the experimental observation: the cells swim easily away from a solid wall but not from a stress-free interface. Moreover when the surface is stress-free, and the initial angle relative to the surface is steep enough, the cell is even trapped at the interface. These results clearly illustrated that the mechanism of the entrapment is the stress-free condition. We thus concluded that the difference of behavior is mainly due to the difference of the stress condition at the interfaces. This conclusion is also supported by the lubrication theory in which large torque is generated for a no-slip interface but no torque is generated in the leading order for a stress-free interface.

Chapter 4

Experiments: Collective motion and coherent structures

4.1 Introduction

Collective motion of organisms is a phenomenon which has frequently attracted the attention of researchers [42, 43], and microorganisms didn't escape this tendency. The ciliates lead to the study of phenomena such as bioconvection patterns [35, 44] of gyrotactic swimmers, or the dancing of *Volvox* [5]. While some other studies reported the collective motion of bacteria and characterized how the correlation of motion between local individuals leads to large scale density fluctuation and coordination even for an organism without cognitive abilities [45, 46]. Such collective motion for bacteria has been explained by the hydrodynamic interactions between pushers while it seems unlikely to happen for other low Reynolds number swimmers [47].

However in preliminary observation we have seen that *Tetrahymena* cells, neutral swimmer as shown in figure 4.1, were showing collective motion at the WAI, movie 3, after day 8 when looking at the cells directly in the petri dish in which the cells were cultivated. Even though not mentioned previously, we observed the cells at the WAI after day 8 when putting them in the PDMS pool first but we didn't observe any collective motion at the time.

In this chapter we will first see how the behavior at the WAI changed when observed

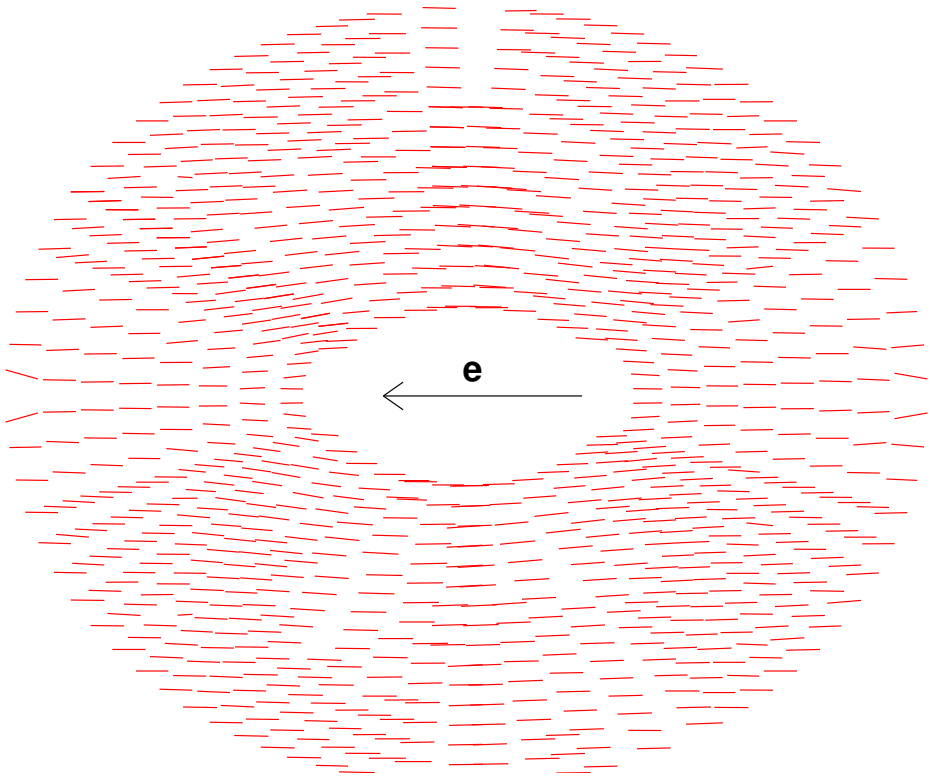

Figure 4.1: Flow field around *Tetrahymena* in the referential of the cell.

directly in the petri dish during the course of 9 days. Then, different plots of correlation values in regard of the distance between cells will give us a preliminary characterization of the motion of the cells. We will briefly compare this collective motion with the collective motion of swimming bacteria. And finally, some observations holding hints of the mechanism of the collective motion are unraveled.

4.2 Methods

In order to observe the behavior of the cells at the water-air interface during the course of nine days, and to observe the collective motion at day 9, we used the set-up shown in figure 4.2. The petri dish in which the cells were cultivated was removed from the

incubator and place directly under microscope. To avoid evaporation, we obtained a 100% humid condition by not removing the lid of the petri dish. For the observation of the behavior of the cells at the WAI, the upright phase contrast microscope (Leica, DM 400B, Germany) coupled with a 10 times objective lens (Leica, HCX PL FLUOTAR 10×/0.30 PH1, Germany) was used. The cells were recorded after 10 minutes, time during which the cells reach a "stable state" of rate entrapment and escape from the WAI. For each type of experiment six different samples inoculated at three different days were used.

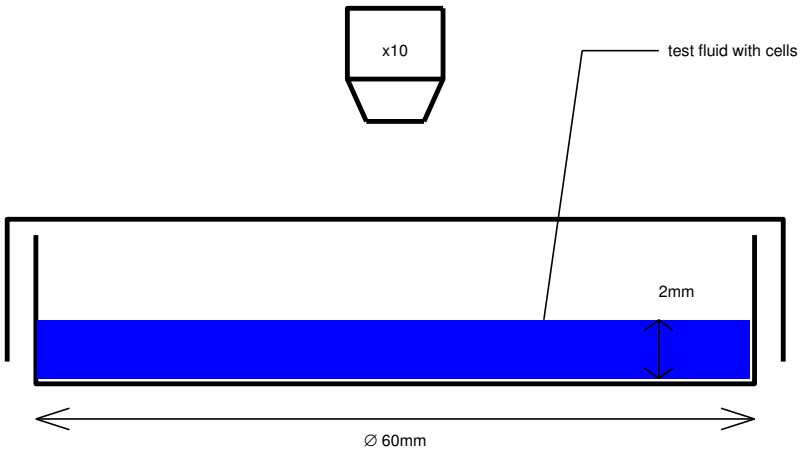

Figure 4.2: Set-up used in order to observe the change of behavior of the cells over the course of nine days, and to observe the collective motion at day 9.

The cells' motion at the interface was recorded by using the high-speed camera (HAS-220, DITECT, Japan) at 50 fps in a window of 860 μm × 640 μm. The trajectories of the extremities were then extracted manually using the plugin MtrackJ on the software ImageJ (http://rsbweb.nuh.gov). This gave us access to the orientation of the cells, as well as their trajectories. The surface concentration of cells was calculated from pictures taken also using the Leica camera (Leica, DFC340 FX) in a window of 1270 μm × 950 μm and then calculated as explained in chapter 2.

To calculate the correlations, multiple videos were taken at 50fps using the DITECT camera. The number of cells at the WAI for each video was then counted and among them, two times six videos were selected so as to have nearly the same number of cells for each group. The trajectories of the extremities of the cells were extracted this time, and it was done so for two consecutive images. The spatial correlations and pair correlation function were calculated as follow using a step of 10 μm.

The pair correlation function was defined as

$$P(r_k) = \frac{1}{N \times A_k \times D} \sum_{i=1}^{N} \sum_{j \neq i}^{N} H(r_k - r_{ij}) H(r_{ij} - r_{k-1}) \tag{4.1}$$

with $k \in \mathbb{N}^*$ (natural integer non equal to zero); $r_k = k \times 10\mu$m; N the number of cells at the WAI in the windows in which the cells were recorded; A_k the area of the crown delimited by the radii r_{k-1} and r_k ($H(x) = 0$ if $x < 0$; $H(x) = 1$ if $x >= 0$); D is the surface concentration of cells at the WAI; r_{ij} if the distance between the cells i and j.

The velocity correlation was defined as

$$\gamma_v(r_k) = \frac{1}{M} \sum_{i=1}^{N} \sum_{j=i+1}^{N} H(r_k - r_{ij}) H r_{ij} - r_{k-1}) \frac{\mathbf{v}_i \cdot \mathbf{v}_j}{|\mathbf{v}_i| \cdot |\mathbf{v}_j|} \tag{4.2}$$

with M is the total number times that the distance separating two cells is between r_{k-1} and r_k; $\mathbf{v}_i$ is the velocity of the cell i and $\mathbf{v}_j$ the velocity of the cell j.

The orientation correlation was defined as

$$\gamma_\theta(r_k) = \frac{1}{M} \sum_{i=1}^{N} \sum_{j=i+1}^{N} H(r_k - r_{ij}) H(r_{ij} - r_{k-1}) \mathbf{e}_i \cdot \mathbf{e}_j \tag{4.3}$$

with M is the total number of times that the distance separating two cells is between r_{k-1} and r_k; $\mathbf{e}_i$ is the orientation of the cell i from bottom to head and $\mathbf{e}_j$ the orientation of the cell j.

And the rotational velocity correlation was defined as

$$\gamma_\omega(r_k) = \frac{1}{M} \sum_{i=1}^{N} \sum_{j=i+1}^{N} H(r_k - r_{ij}) H(r_{ij} - r_{k-1}) \mathbf{z}\omega_i \cdot \mathbf{z}\omega_j \tag{4.4}$$

with M is the total number times that the distance separating two cells is between r_{k-1} and r_k; $\mathbf{e}\omega_i$ is the normalized rotational velocity of the cell i and $\mathbf{z}\omega_j$ the normalized

rotational velocity of the cell j. $\mathbf{z}\omega$ is a unit vector in the direction normal to the WAI and of value ± 1 depending if the orientation vector of the cell is turning clockwise or anti clockwise between the two successive images from which it was extracted.

4.3 Results and discussion

Since we observed the collective motion of cells after the day 7, we first characterized once again the behavior of cells at the WAI with the passing days. But it was done so for nine days this time, and while looking at the cells directly in the petri dish in which they were cultivated.

4.3.1 Behavior at the WAI in petri dish

To characterize the behavior of the cells we monitored the change of the velocity and number of cells at the WAI. Figure 4.3(A) shows how the total concentration of cells in the medium changes during 9 days as a reference to make sure that this parameter didn't change from the one presented in the figure 2.8(A) of chapter 2. If the total concentration does not appear to have change much, when comparing figure 4.3(B) and 2.8(B) of chapter 2 it appears that less cells are at the WAI in the fifth day in the case of the petri dish than in the case of the PDMS pool. This difference can easily be recognized when looking at the pictures of the cells at the WAI in figure 4.4 and the one in figure 2.11.

Figure 4.5 shows how the swimming velocity of the single cells at the WAI changes during nine days when observed directly in the petri dish of culture. Their swimming velocity gradually increases from $\sim$50 μm.s^{-1} at day three to $\sim$230 μm.s^{-1} at day nine after the sudden drop of velocity from day one to day 3. All in all, it appears than the velocity of the cells in the petri dish is lower than the one in the PDMS pool, figure 2.9(B). However, the velocity in the PDMS pool was taken from a diluted suspension as explained in chapter 2 while the velocity in the petri dish could not be taken from a diluted suspension since the collective motion observed at day 9 would disappear when the cells are removed from their original petri dish. The velocity was therefore measured by selecting the cells with no neighbor within a radius of a body size as shown in figure 4.6. It is still interesting to remark that as the days go by, the velocity of the cells increases remarkably and constantly up to day 9 when the collective motion is observed.

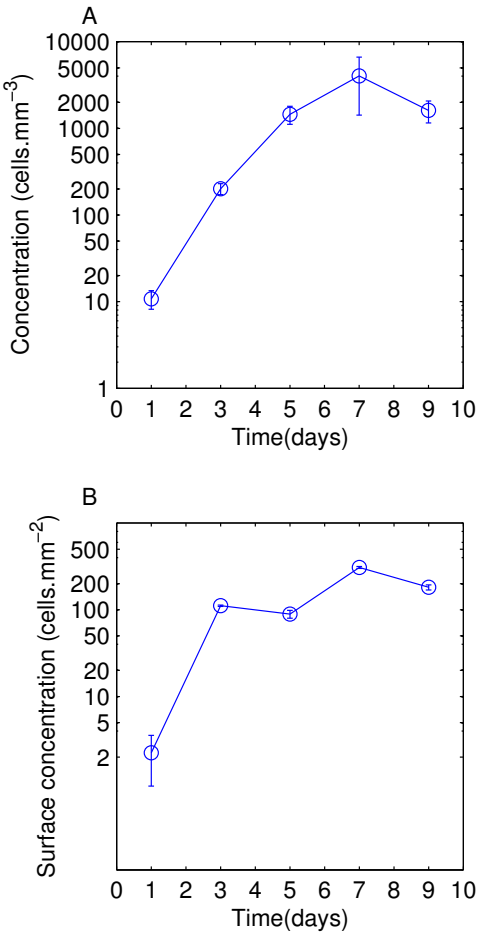

Figure 4.3: Change of the concentrations of cells over the course of nine days every two days. The graphs have a semi-log y-axis. The error bars indicate the standard deviation. (A) Volume concentration inside the medium. It increases from 10 cells.mm^{-3} to 2000 cells.mm^{-3} during the first five days after inoculum. On the fifth day, it reaches almost a plateau phase that lasts up to the ninth day. (B) Surface concentration at the water-air interface. It presents a first growth phase from 2 cells.mm^{-2} to $\sim$100 cells.mm^{-2} that ends at the third day, and is also followed by a first plateau at $\sim$100 cells.mm^{-2} until the fifth day. Before rising toward a second plateau at $\sim$200 cells.mm^{-2} from the seventh day to the ninth day. We can observe here a first difference of entrapment characteristic at the WAI with the case of chapter 2 when the cells were transferred in a PDMS pool.

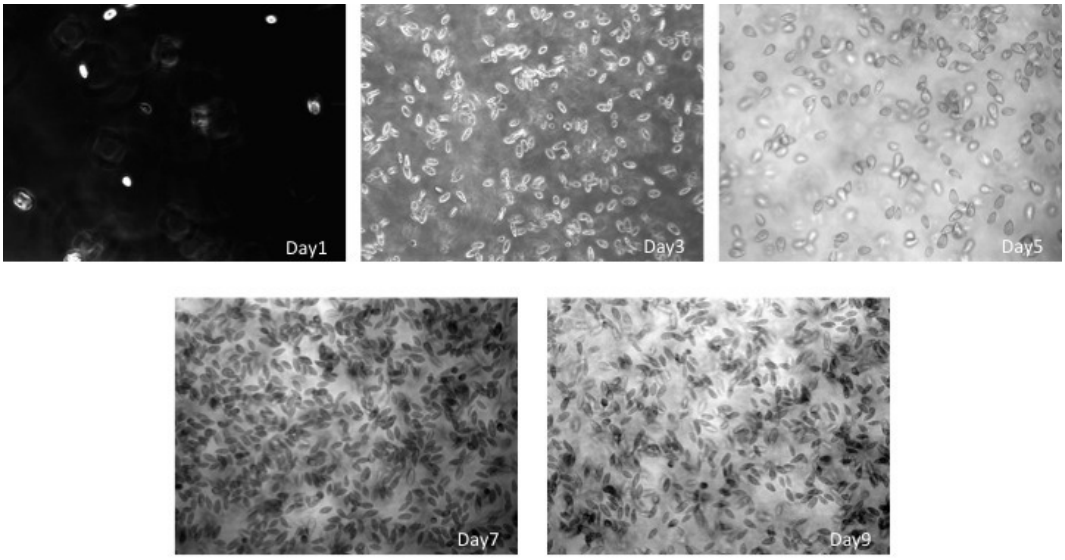

Figure 4.4: Example of cells being trapped at the WAI over the course of nine days when observed directly in the petri dish.

Since we confirmed a change in behavior at the WAI when the cells are observed in the petri dish of culture and when they are observed in a PDMS pool, we tried to characterize the collective motion by measuring different correlation values in function of the distance between cells at day 9, that is when the collective motion could be observed.

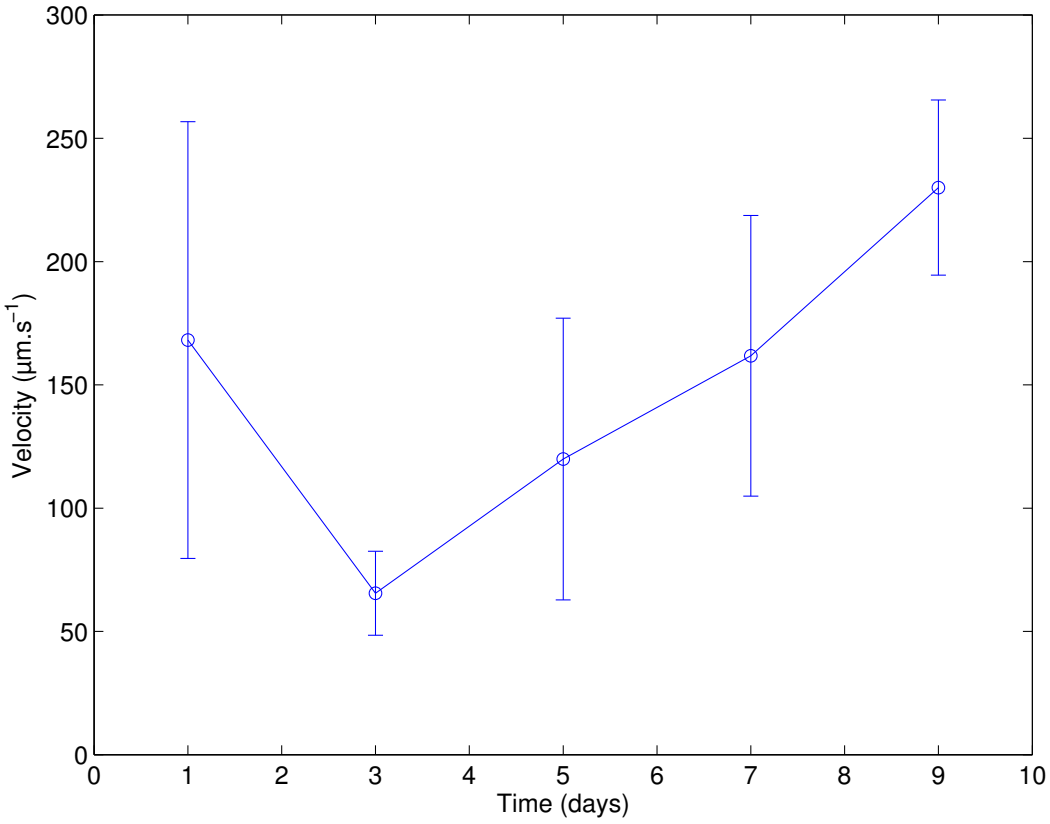

Figure 4.5: Change of swimming velocity of cells over the course of nine days at the WAI. The axes of the graphs are both linear. The cells still swim at 1/3 or less of the velocity at which they swim away from any interface. However they also seem to be swimming slower than the single cells in the PDMS pool, and their speed gradually increases from $\simeq$50 μm.s^{-1} at day three to $\simeq$230 μm.s^{-1} at day nine.

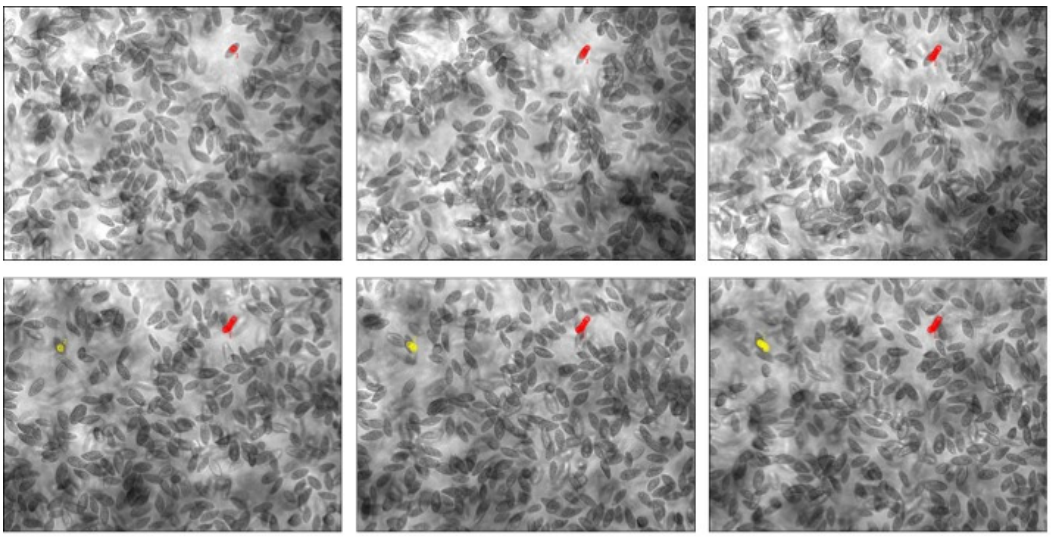

Figure 4.6: Example of two cells being tracked. They have been chosen so that no other cells at the WAI are within a perimeter of one body length.

4.3.2 Characterization of collective motion

In order to characterize the collective motion of cells, it is usual to consider the pair correlation function, spatial orientation correlation and spatial velocity correlation [48]. To which we added rotational velocity correlation to check how the relative alignment between cells tried to stay coherent in time. These parameters have been extracted for two different values of number of cells at the WAI, $\sim$520 cells.mm^{-2} and $\sim$220 cells.mm^{-2}.

Figure 4.7 shows the pair correlation function. At low density, there is a big and large spike of the correlation at $\sim$35 μm and of $\sim$40 μm width. The high density also have a spike, but of a lower value, and half of the width of the low density spike. Even though it could seem surprising at first, the lower surface concentration appears to have a structure that last on longer scales. However, if we take into account the fact that the maximal surface concentration on the WAI that can be obtained is $\sim$1270 cells.mm^{-2}, it is less surprising that for the surface concentration of $\sim$520 cells.mm^{-2}, which is half of the maximum density, the pair correlation function quickly lowers to 1 as the distance separating cells increases since half of the windows is covered with cells. On the other hand the fact that the pair correlation function stays higher than 1 for a large distance in the case of the lower surface concentration indicates that cells tends to be at the WAI as small groups instead of being homogeneously distributed. We can observe these two different types of distribution in figure 4.8.

The spatial orientation correlation can be observed in figure 4.9. For the lower density, the orientation correlation decreases from 0.25 to 0 over $\sim$70 μm while for the higher density it decreases from 0.2 to 0 over $\sim$50 μm. Even though in both cases the correlation is lost over about one body length, the higher surface concentration has a lower correlation and looses this correlation on shorter distances than the low surface concentration. This can be somehow related to the density probability since it suggests that at lower density, cells appear to gather more easily into small groups than in the case of high density where there is not enough free space to allow such repartition.

On figure 4.10, the spatial velocity correlations for the two surface densities can be observed. We can clearly observe a spatial persistence in the velocity correlation of cells over about 1.5-body length (3 body widths), which coupled with the one of the spatial orientation correlation, confirms the presence of a collective motion at day 9. The main difference between these two correlations lays in the possibility for the lower density to

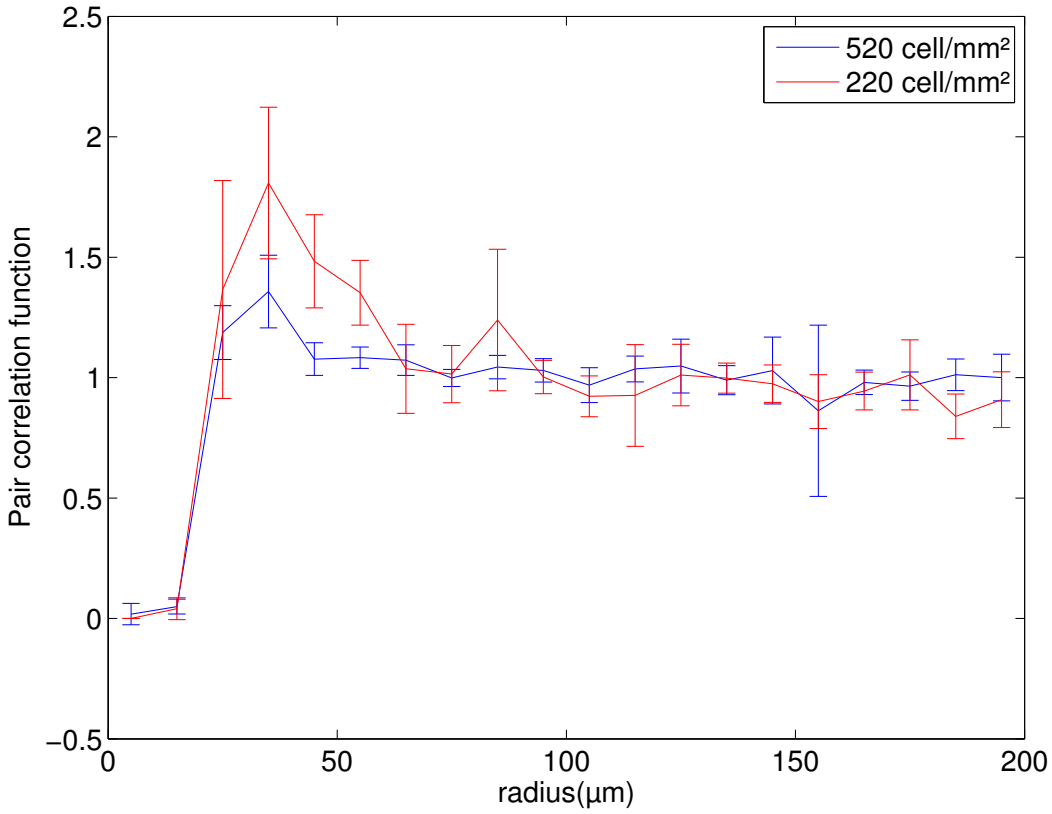

Figure 4.7: Pair correlation function with 220 and 520 cells.mm^{-2}

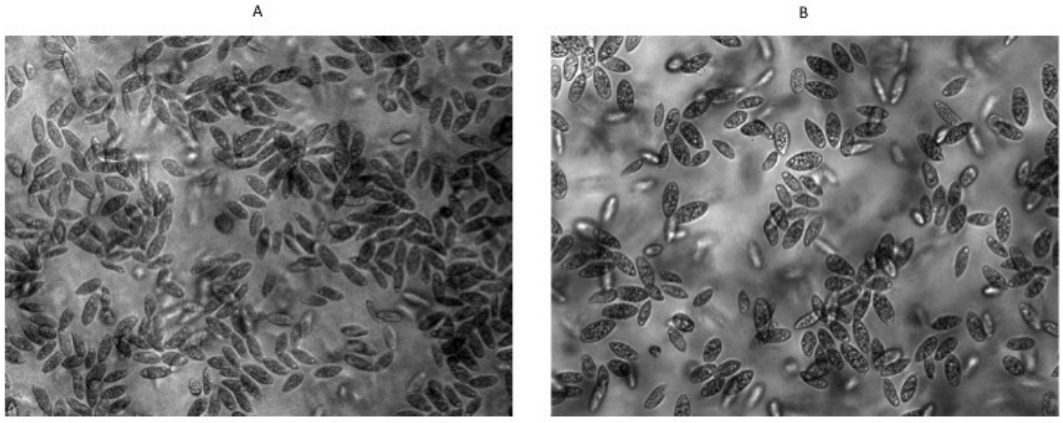

Figure 4.8: Example of the distribution of cells at the WAI for two surface densities of cells: (A) $\simeq$520 cells.mm^{-2}, (B) $\simeq$220 cells.mm^{-2}.

have negative correlation at large distances. If taking into account the spatial density probability, we can understand this difference by the fact that for the lowest density, the cells swim while being in groups, and, from the left part of the figure 4.10, they do so in small groups. Movie 4 could lead us to think that the cells are not free swimmers anymore but point forces at the WAI, therefore disturbing the medium around them on large scale by inducing local flow. A larger distance between groups may allow a coordination of global flow making the groups preferably swimming in a specific direction, while at higher density the presence of such global flow is prevented as the correlation of the cells suggests it by the loss of orientation correlation on shorter distance. Therefore, in higher density the direction of velocity is easily more random than in the lower density case, which could explain why the correlation stays at zero at high density for large distance while it doesn't at low density.

Interestingly, even though these three previous plots indicate a spatial persistence of collective swimming, the figure 4.11 seems to indicate that the cells don't instantaneously rotate accordingly to their neighbors. However the persistent orientation correlation suggests that over time the rotation should be coordinated. But the type of equation used

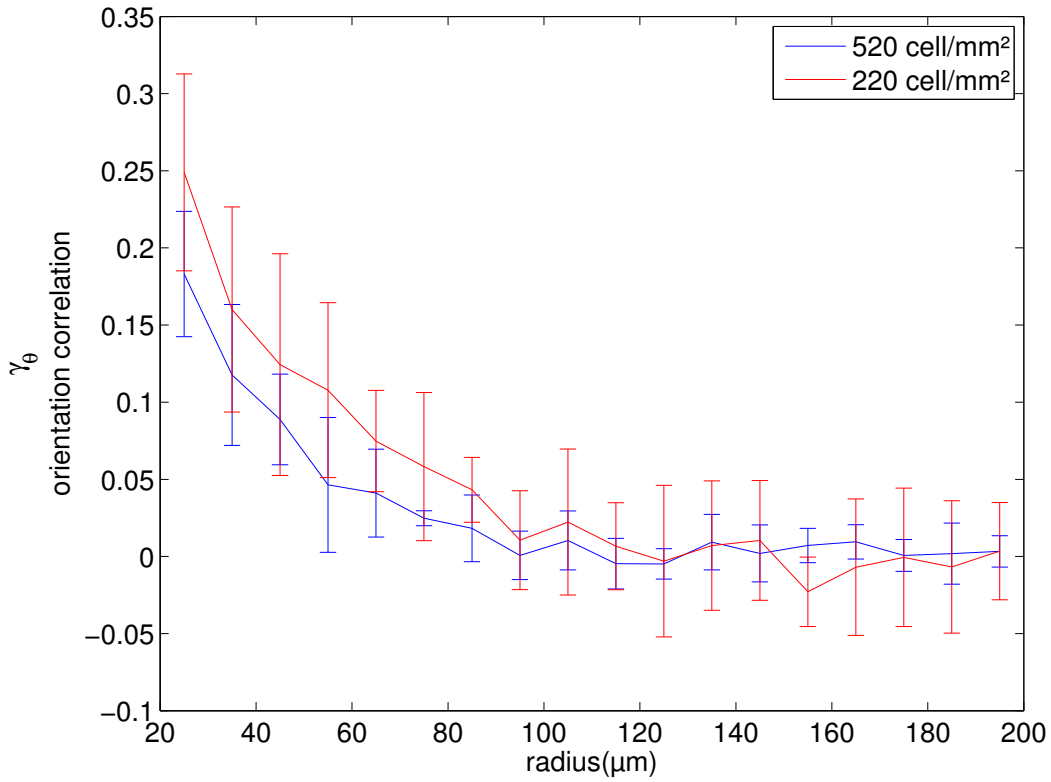

Figure 4.9: Orientation correlation of cells with 220 and 520 cells.mm^{-2}.

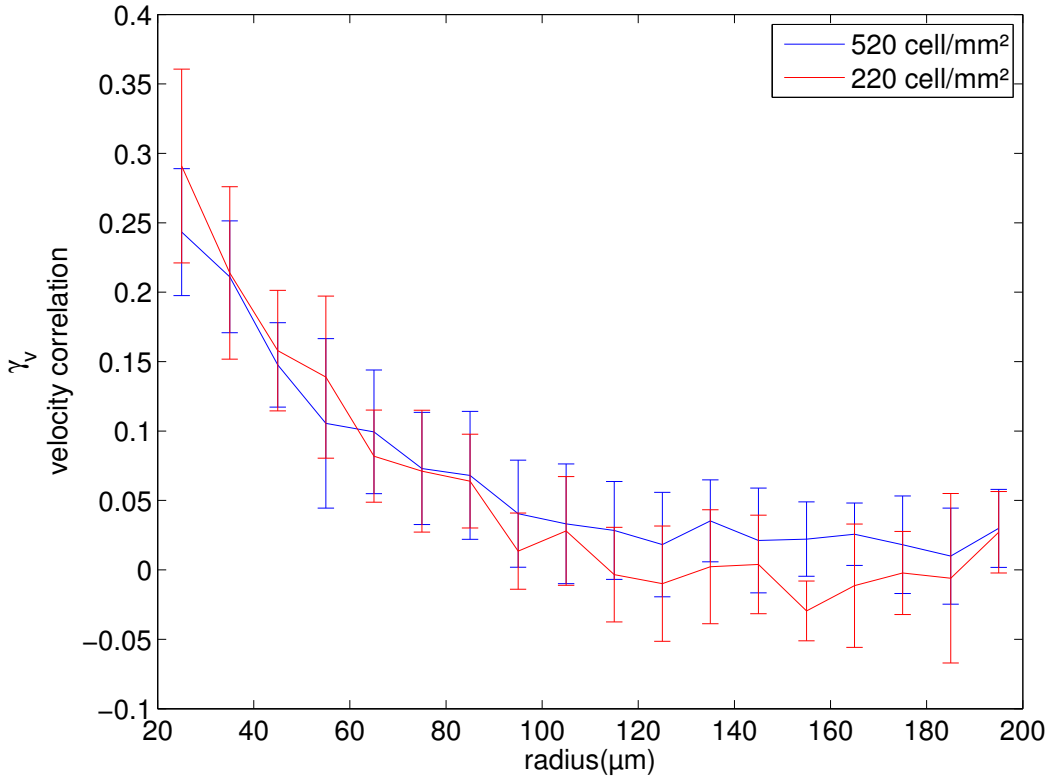

Figure 4.10: Velocity correlation of cells with 220 and 520 cells.mm^{-2}.

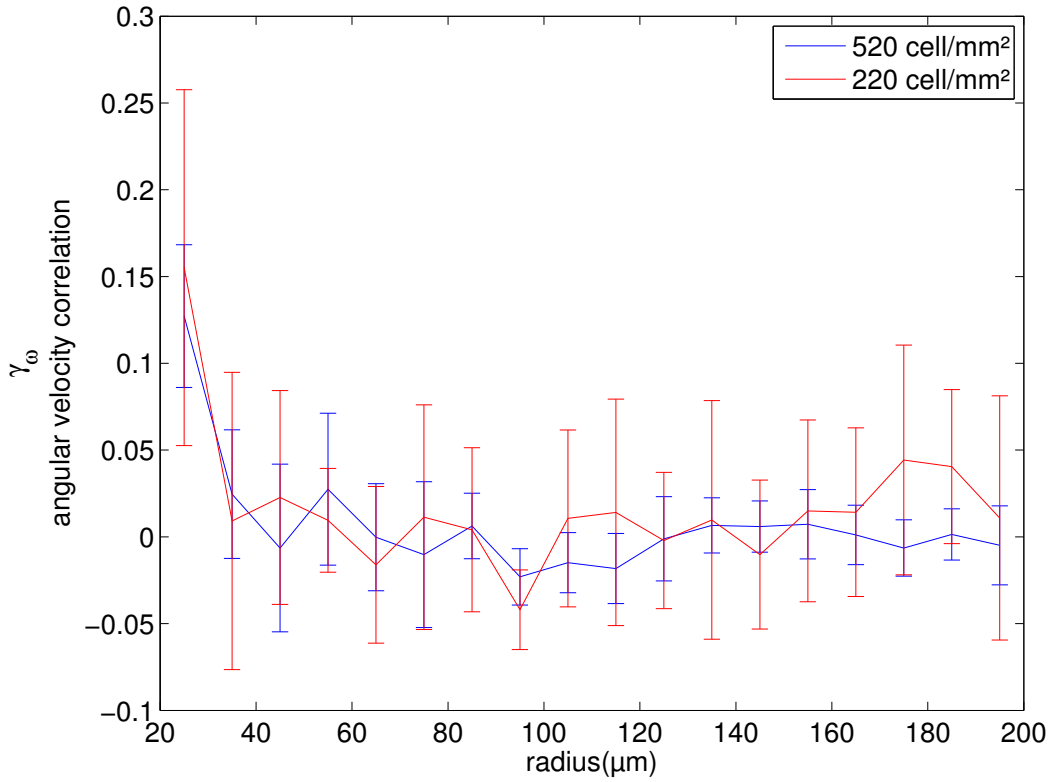

Figure 4.11: Rotational velocity correlation with 220 and 520 cells.mm^{-2}.

here may not be adequate to perform an effective analysis of the situation. The equation used to calculate rotational velocity does not take into account the amplitude of the rotation but only the sign of rotation that can explain why the correlation decreases so quickly. It is therefore difficult to correctly link this correlation to the previous ones.

4.3.3 Comparison with collective motion of swimming bacteria

In their respective works, both Christopher Dombrowski [49] and Takuji Ishikawa [50] showed that bacteria present collective motion at high concentration, while not discussing the low concentration case. This motion is characterized by a high value, and persistently non-equal to zero over tens of body lengths for the value of the spatial velocity correlation. On the other hand, not only does the velocity correlation of *T.thermophila* have a lower value, but also it is persistently non-equal to zero over about two body lengths (four body widths). Such a simple comparison reveals that even though these two organisms are swimmers, their collective motion appears to be of a different nature.

4.3.4 Discussion

The cells don't accumulate at the WAI in a same manner when in a petri dish and when a PDMS pool. In some preliminary observation, not reported here, we also realized that the collective motion could only be observed in the petri dish in which the cells were cultivated. That is even when we poured the cells in another petri dish, we could not observe the cells collective motion at the WAI anymore, but it could be observed again instantaneously when the cells when poured back in the original petri dish. This gave us a hint that some surface related chemicals could play a role in the inducing of the collective motion behavior. We decided then to check again some data from the chapter 2 to see if the addition of surfactant in a medium containing five days old cells in a PDSM pool could induce them into collective motion. As shown in movie 5, when having $\sim$0.04mM.m^{-3} of Tween20 with the cells, they appear to present a collective motion. For such amount of surfactant the swimming velocity of the cells is also increased to $\sim$450 μm.s^{-1} as shown in figure 2.15(B) in chapter 2. Even though on the movie 3 the cells appear to move faster than in movie 6, when we compare the swimming velocity at day 9, $\sim$230 μm.s^{-1}, with the one with the right amount of surfactant to have collective motion, $\sim$450 μm.s^{-1}, it seems like the velocity may not play an important role in the collective motion.

However, the velocity of cells at day 5 with surfactant was taken from a diluted suspension as explained in chapter 2 while the velocity at day nine could not be taken from a diluted suspension since the collective motion disappear when the cells are removed

from their original petri dish. The velocity was therefore measured by selecting the cells with no neighbor within a radius of a body length as shown in figure 4.6. It is then not easy to affirm that the speed of a single cell in a medium is lower than in the diluted case because of the entrapment itself or because of the effect of the neighbors. As a matter of fact, movie 4 reveals that the cells are not free swimmers anymore but produce jet flows. Therefore they can generate a flow that will decay on a larger scale, and by doing so, they can affect the motion of the fluid on larger scale than a cell body. Hence hindering the cells that seem to be without close neighbors as shown in figure 4.6. The swimming velocity of the cells should then still be considered as one of the possible parameter necessary to obtain collective motion at the WAI.

As for the drop of velocity in a petri dish when compared to the one in PDMS pool, in addition of the previous argument about possible flow created by the other cells in the medium, as explained earlier, some additional chemicals seem to be lost when cells are removed from the petri dish of culture. It is therefore difficult at this stage to make any strong conclusion on the most likely reason which could explain the decrease of velocity at the WAI in a petri dish in opposition to a PDMS pool and, for the matter at hand, how this could play a role in inducing the cells to present a collective motion. When comparing the images in figure 4.4, one could assume that the shape of the cell could be a key parameter in inducing the collective motion, but since five days old cells can present a collective motion when surfactant is added, it is once again not obvious how important is the shape of cells for the collective motion. Finally, we have seen that the surface concentration of cells affect the parameters describing the collective motion, but the mechanism behind the collective motion itself not having yet been solved, it is difficult to make clear conclusion of the importance of surface concentration in inducing collective motion.

It is however interesting to remark that, when comparing our results to previous study about collective motion, the behavior of *T.thermophila* is closer to a near-field collision driven collective motion of neutral swimmers such as the one described by Shashi Thutupalli [51], than the swarming of bacteria studied by Takuji Ishikawa [50] and Christopher Dombrowski [49]. The length scale of the correlation reported, about three body lengths for the artificial neutral swimmer, and about tens of body lengths for the bacteria suggest that we are in front of a collision driven phenomena instead of a far field interaction. But,

the cells swimming side by side for a short amount of time, suggest that the collision are not elastic but need some time for the reorientation of the cells.

The collective motion could be due to the free swimmer producing jet flow at the WAI, to the presence of some chemical allowing the cells to swim more freely than the ones at day five, to the swimming velocity (possibly related to the chemicals), and/or to the shape of the cells or/and the surface concentration. However, it is clear that the nature of the collective motion in this case is different from the one in the case of bacteria.

4.4 Summary

In this chapter we have reported for the first time, at the author's knowledge, the collective motion of neutral swimmers in a biological system, which was not predicted by former theories. When characterizing this collective motion phenomenon at day nine, for both high and low surface densities, the spatial correlations of the velocity and orientation confirm the presence of a collective behavior. The nature of collective motion of *T.thermophila* is different than the one of bacteria, and the difference may come from the individual swimming motion whether the cell is a pusher or a neutral swimmer.

Chapter 5

Conclusions

In recent years, physics provided to the study of the behavior of microorganisms a new approach. In particular the use of fluid mechanics allows to explain complicated phenomena such as bioconvection, and entrapment of bacteria close to a solid. In this thesis, we report and characterize the novel entrapment phenomenon of ciliates at the water-air interface, and use physics approach to explain the mechanism behind it.

5.1 Conclusion

In chapter 2, we characterize the novel entrapment phenomenon of *T.thermophila* at the water-air interface and investigated wether the mechanism is mainly due to biology or physics. And in chapter 3, in order to clarify the mechanism of entrapment more in detail, we numerically investigated the behavior of a squirmer close to stress-free interface and a solid wall. In chapter 4, we report their collective motion of at the interface. A summary and conclusion of this thesis are presented below.

In chapter 2, the changes of behavior, swimming velocity and surface concentration, of *T.thermophila* at the water-air interface and inside the medium away from solid and water-air interfaces were compared. It appears that at the interface the cells are swimming at $\sim$200 μm.s^{-1} , that is about 1/3 of the swimming velocity inside the medium. To narrow the possible causes of the entrapment, two sets of experiment were conducted. In the first

one, the relation between the entrapment and the taxes that cause higher concentration of cells close to the WAI was tested. No significant change of behavior was observed when modifying the conditions related to the geotaxis and aerotaxis. Therefore, we discarded the possibility of these taxes being the causes of the entrapment. On the other hand, the modification of the physical properties at the WAI, surface tension and mobility of fluid particle, resulted in a sudden loss of the entrapment when enough surfactant was added. It also appears like at an intermediate value of surfactant addition, the swimming velocity of the cells at the WAI doubles. In light of the different experiments, we concluded that the mechanism behind this novel entrapment phenomenon lies in the interfacial physics.

In chapter 3 we clarified the mechanism of entrapment using a numerical simulation of the motion of a squirmer close to a stress-free interface and a solid wall. After doing some scaling, we considered the stress-free interface as flat. Using the BEM analysis, we found that when the swimmer is going towards a solid wall, a strong torque is applied on it by the lubrication flow, and it orientates away from the wall. On the other hand, such a big torque is not present in the case of the stress-free interface. As a result it takes a lot more time to the cell to orientate away from the interface, which seems consistent with the experimental observations. Moreover, the cell is actually trapped at the interface, when the surface is stress-free and the initial angle is enough steep to the interface. Such a finding indicates that the stress-free boundary condition is the main mechanism of the entrapment.

In the chapter 4, we have reported the collective motion of the neutral swimmer at the WAI, though it was not predicted by any of former theories. To the best of our knowledge it is the first that collective motion in biological system was observed. When characterizing this collective motion phenomenon at day nine for both high and low surface densities, the spatial correlations at the velocity and orientation confirm the presence of a collective behavior. The nature of collective motion of *Tetrahymena* is different from the one of bacteria, and the difference may come from the individual swimming motion whether the cell is a pusher or a neutral swimmer.

The main interest raised by this thesis is the study of the novel entrapment phenomenon of ciliates at the water-air interface. Taking into account the possible effect of ciliates at

the WAI, such as the change the gas rate exchange between air and water, or modification of the mixing of nutrient close to the WAI. This thesis can open a new field in the study of microorganisms at interfaces.

5.2 Prospect

The work performed during this thesis may lead to many future works, as should any new phenomenon do.

1. The mechanism of entrapment:

We have seen that we could explain the mechanism of entrapment at the WAI simply as a matter of weakness of torque originated from the interaction of stress field around the cells with the WAI. However some work conducted on the entrapment of bacteria at the WAI [52] explain it by the hydrophobicity of the cell. We therefore need to check whether this phenomenon is important of not.

2. Other ciliates:

We have observed this entrapment for *Tetrahymena thermophila*, and from our model, we would expect the same result to be observed for cells such as *Paramecium*. In addition of verifying if it would be the case, it would be interesting to look into the case of other ciliates or neutral swimmers.

3. Nutrient mixing and collective motion:

As we have seen in the movie 4, the trapped cells seem to increase the mixing at the WAI. But if we take into account how a *Volvox* creates a flow downward when close to a cover slip due to the impossibility for the cell to go further upward (cf fig. 1.12), we could expect such a flow also for a ciliate trapped at the WAI. In which case, the mixing would not be enhanced only at the WAI but close to the WAI in general. Ishikawa et al. [50] has shown how collective motion of bacteria enhances mixing. It would be also interesting here to study such a relation.

4. Effects of ciliates on the medium:

The presence of ciliates at the WAI itself could modify the gas rate exchange between

the air and the medium; they could stabilize or destabilize an emulsion and so on. It would be interesting to see how ciliates trapped at an interface would change the physical properties of the system in which they are present.

5. Surfactant:

When enough is added to the interface, the ciliates escape easily from the WAI. If taking into account the numerical study, this could result from a Marangoni flow. It would be first interesting to verify if this is really the case, and how in lower concentration they affect the entrapment exactly. This could lead to a better understanding of the interaction between human and nature, and better mean to prevent pathogen ciliates to stay at the WAI in sewage water.

6. Medical application:

The presence of ciliated cells close to stress-free interface is not limited to microorganism. In the airways, as an example, it is easy to find epithelial ciliated cells in presence of interfaces at least between liquids if not between water and air. The understanding of the interaction of ciliated microorganisms with stress-free interfaces could be applied in order to have a better understanding of both the mucus transport in the body and the diseases associated to it.

Bibliography

[1] Kristiansen T.B., Hagemeister J.J., Grave M., Hellun-Larsen P., Surface mediated death of unconditioned *Tetrahymena* cells: elleft of physical parameters, growth factors, hormones, and surfactants, J. Cell Physiol., 169 (1996) 139-148.

[2] Neu T.R., Significance of bacterial surface-active compounds in interaction of bacteria with interfaces, Microbiol. Rev., 60 (196) 151-166.

[3] Glassman H.N., Surface active agents and their application in bacteriology, Bacteriol. Rev., 12 (1948) 105-148.

[4] Giacché D., Ishikawa T., Yamaguchi T., Hydrodynamic entrapment of bacteria swimming near a solid surface, Phys Rev E Stat Nonlin Soft Matter Phys., 82 (2010) 056309.

[5] Drescher K., Leptos K.C., Tuval I., Ishikawa T., Pedley T.J., Goldsein R.E., Dancing Volvox: Hydrodynamic Bound States of Swimming Algae, Phys. Rev. Lett., 102 (2009) 946-952.

[6] Lauga E., Diluzio W.R., Whitesides G.M., Stone H., Swimming in circles: Motion of bacteria near solid boundaries, Biophys. J., 90 (2006) 400-412.

[7] Frymier D.F., Ford R.M., Berg H.C., Cummings P.T., Three-dimensional tracking of motile bacteria near a solid planar surface, Proc. Natl. Acad. Sci.USA, 92 (1995) 6195-619

[8] Hartcher R.F., ParkerB.C., Microbiological and chemical enrichment of freshwater-surface microlayers relative to the bulk-subsurface water, Can. J. Microbiol., 20 (1974) 1051-1057.

[9] Norkrans B., Surface microlayers in aquatic environments, Adv. Microb. Ecol., 4 (1980) 51-85.

[10] Zaitsev.Yu.P. , Marine neustonology, K. A. Vinogradov, Jerusalem (1971).

[11] Gladyshev M. I. , Biophysics of the surface microlayer of aquatic ecosystems, IWA Publishing, Cornwall (2002).

[12] Cunliffe M., Upstill-Goddard R.C., Murrell J.C., Microbiology of aquatic surface microlayers, FEMS Microbio. Rev., 35 (2011) 233-246.

[13] Duchemin L., Popinet S., Josserand C., Zaleski S., Jet formation in bubble bursting at a free interface, Phys. Fluids, 14 (2002) 3000–3008.

[14] Blanchard D.C., Syzdek L.D., Concentration of bacteria in jet drops from bursting bubbles, J. Geophys. Res., 77 (1972) 5087–5089.

[15] Jaenicke R., Matthias-Maser S., Gruber S., Omnipresence of biological material in the atmosphere, Env. Chem., 4 (2007) 217–220.

[16] Casareto B.E., Suzuki Y., Okada K., Morita M., Biological micro-particles in rain water, Geophys. Res. Let., 23 (1996) 173–176.

[17] Burge H., Bioaerosols: Prevalence and health effects in the indoors environment, J. of Allergy and Clinical Immuno. 86 (1990) 687–701.

[18] Lee W.L., Jayathilake P.G., Tan Z.J., Le D.V., Lee H.P., Khoo B.C., Muco-ciliary transport: effect of mucus viscosity, cilia beat frequency and cilia density, Computer & Fluids. 49 (2011) 214–221.

[19] Smith D.J., Gaffney E.A., Blake J.R., Modeling mucociliary clearance, Resp. Physio. Neurobio., 163 (2008) 178–188.

[20] Blanchetti R., Erra F., The ethology of protozoa and the "adaptative space" hypothesis: a heuristic approach to the biology of these eukaryotic, unicellular organisms, Protist, 3 (2003) 58–68.

[21] Coyne R.S., Tetrahymena, eLS. (2011)

[22] Kathleen C., *Tetrahymena thermophila*, Method in cell biology, 10, Elvesier, Berkeley (2012) .

[23] Lighthill M.J., On a squirming motion of nearly spherical deformable bodies through liquids at very small reynolds number, Comm. Pure Appl. Math., 5 (1952) 109–118.

[24] Blake J.R., A spherical envelope approach to ciliary propulsion, J. Fluid Mech., 46 (1971) 199–208.

[25] Magar V., Goto T., Pedley T.J., Average nutrient uptake by self-propelled steady squirmer, J. Fluid Mech., 539 (2005) 93-112.

[26] Evans A.A., Ishikawa T., Yamaguchi T., Lauga E., Orientational order in concentrated suspension of spherical microswimmers, Phys. Fluids, 23 (2011) 111702.

[27] Llopis I., Pagonabarra I., Hydrodynamic interactions in a squirmer motion: swimming with a neighbor and close to a wall, J. Non-Newton. Fl. Mech., 165 (2010) 946-952.

[28] Blake J.R., A note on the image system for a stokeslet in a no-slip boundary, Proc. Camb. Phil. Soc., 70 (1971) 303-310.

[29] Blake J.R., Action of a force near the planar surface between two semi-infinite immiscible liquids at very low Reynolds numbers, Bull. Austral. Math. Soc., 18 (1978) 345-356.

[30] Riedel I.H., Kruse K., Howard J., A self-organized vortex array of hydrodynamic ally entrained sperm cells, Science, 309 (2005) 300-303.

[31] Spagnolie S.E., Lauga E., Hydrodynamic of self propulsion near a boundary: predictions and accuracy of far-field approximations, J. Fluid Mech., 700 (2012) 105-147.

[32] Crowdy D., Lee S., Samon O., Lauga E, Hosoi A.E., A two-dimensional model of low-Reynolds number swimming beneath a free surface, J. Fluid Mech., 681 (2011) 24-47.

[33] Gavin L. and Gillian D.L., Microbial Biofilms: Current Research and Applications, Caister Academic Press, Portland (2012).

[34] Fangliang Wu C., Biofilm formation and its interaction with surfactants and solvents [electronic resource] : a physico-biological approach, Stanford University, Department of Chemical Engineering (2012).

[35] Hill N.A., Pedley T.J., Kessler J.O., Growth of bioconvection patterns in a uniform suspension of gyrostatic micro-organisms in a layer of finite depth, J. Fluid Mech., 195 (1988) 223–237.

[36] Ishikawa T., Simmonds M. P. and Pedley T. J., Hydrodynamic interaction of two swimming model micro-organisms, J. Fluid Mech. 568 (2006) 119–160.

[37] Asai D. J., Rajagopalan V., and Wilkes D. E., Dynein-2 and Ciliogenesis in *Tetrahymena*, Cell Motility and the Cytoskeleton, 66 (2009) 673–677.

[38] White Frank, Viscous fluid flow second edition, McGraw-Hill (1991).

[39] Ishikawa T., Yamaguchi T., Shear-induced fluid-tracer diffusion in a semidilute suspension of spheres, Phys. Rev. E, 77 (2008) 041402.

[40] Lima R., Wada S., Tsubota K., Yamaguchi T., Confocal micro-PIV measurements of three-dimentional profiles of cell suspension flow in a square microchannel, Measurement Science and Technology, 17 (2006) 797-808.

[41] Short M.S., Solari C.A., Ganguly S., Powers T.R., Kessler J.O., Flows driven by flagella of multicellular organisms enhance long-range molecular transport, Proc. Natl. Acad. Sci. USA., 103 (2006) 8315-8319.

[42] Ballerini M., Cabibbo N., Candelier R., Cavagna A., Cisbani E., Giardina I., Lecomte V., Oriandi A., Parisi G., Procaccini A., Viale M., Zdravkovic V., Interaction ruling animal collective behavior depends on topological rather than metric distance: Evidence from a field study, Proc. Natl. Acad. Sci. USA, 105, (2007) 1232–1237.

[43] Couzin I.D., Krause J., Self-organization and collective behavior in vertebrates, Adv. Stud. Behav., 32 (2003) 1-75.

[44] Mogami Y., Yamane A., Gino A., Baba S.A., Bioconvection pattern formation of *Tetrahymena* under altered gravity, J. Exp Biol., 207 (2004) 3349–3359.

[45] Zhang H.P., Avraham Be'er, Florin E.L., Swinney H.L., Collective motion and density fluctuations in bacterial colonies, Proc. Natl. Acad. Sci. USA, 107 (2010) 13626-13630.

[46] Sokolov A., Aranson I.S., Kessler J.O., Goldstein R.E., Concentration dependence of the collective dynamics of swimming bacteria, Phys. Rev. Lett., 98 (2007) 158102

[47] Saintillan D, Shelley M.J., Emergence of coherent structures and large-scale flows in motile suspensions, J. R. Soc. Interface 9 (2012) 571-585.

[48] Vicsek T., Zafeiris A., Collective motion, Physics reports, 517 (2012), 71-140.

[49] Dombrowski C., Cisneros L., Chatkaew S., Golstein R.E., Kessler J.O., Self-concentration and large-scale coherence in bacterial dynamics, Phys. Rev. Lett., 93 (2004), 098103.

[50] Ishikawa T., Yoshida N., Ueno H., Wiedeman M., Imai Y., Yamaguchi T., Energy transport in a concentrated suspension of bacteria, Phys. Rev. Lett. 107 (2011) 028102.

[51] Thutupalli S., Seeman R., Herminghaus S., Swarming behavior of simple model squirmers, N. J. Phys. 13 (2011) 073021.

[52] Schäfer A., Harms H., Zehnder A.J.B., Bacterial accumulation at the air-water interface, Environ. Sci. Technol., 32 (1998) 3704-3712.

Appendix A

Movies captions

Movie1: *T.thermophila* trapped at the WAI and observed in the set-up shown in figure 2.16. The movie was recorded at 1000 fps and is displayed at 30 fps.

Movie2: *T.thermophila* trapped at the strait WAI and observed in the set-up shown in figure 2.7. The movie was recorded at 1000 fps and is displayed at 30 fps.

Movie3: Collective motion of cells at the WAI at day 9 when observed in the petri dish as shown in figure 4.2. The movie was recorded and is displayed at 30 fps.

Movie4: Mixing induced by the cells when trapped at the WAI. The movie has been recorded in dark field with 1 μm diameter beads. The movie was recorded and is displayed at 30 fps.

Movie5: Collective motion at the WAI observed at day 5 in a PDMS pool when enough surfactant Tween20 is added. The movie was recorded and is displayed at 20 fps.

Movie6: Cells trapped at the WAI at day 5 in a PDMS pool. The movie was recorded and is displayed at 20 fps.

List of publications

Journal paper

[1] Jonathan Ferracci, Hironori Ueno, Keiko Numayama, Yohsuke Imai, Takami Yamaguchi, Takuji Ishikawa, Entrapment of fresh water ciliates at the water-air interface, Phys. Rev. Lett., submitted.

[2] Jonathan Ferracci, Hironori Ueno, Keiko Numayama, Yohsuke Imai, Takami Yamaguchi, Takuji Ishikawa, Numerical simulation of entrapment of a squirmer at the water-air interface, Phys. Rev. E, in preparation.

[3] Jonathan Ferracci, Hironori Ueno, Keiko Numayama, Yohsuke Imai, Takami Yamaguchi, Takuji Ishikawa, Collective motion of fresh water ciliates trapped at the water-air interface, Phys. Rev. E, in preparation.

Conference paper

[1] Jonathan Ferracci, Takuji Ishikawa, Hironori Ueno, Keiko Numayama, Yohsuke Imai, Takami Yamaguchi, Entrapment of fresh ciliates at the interface fluid-air, 5^{th} East Asian Pacific Student Workshop on Nano-Biomedical Engineering, pp 120-121, December 2011

[2] Jonathan Ferracci, Hironori Ueno, Keiko Numayama, Yohsuke Imai, Takami Yamaguchi, Takuji Ishikawa, Hydrodynamic entrapment of ciliates at the air-fluid interface, Proceeding of Biological Complex Fluids Softflow 2012, pp 36-37, June 2012

[3] Jonathan Ferracci, Hironori Ueno, Keiko Numayama, Yohsuke Imai, Takami Yam-

aguchi, Takuji Ishikawa, Hydrodynamic entrapment of ciliates at the air-fluid interface, Bulletin of American Society 65^{th} Annual meeting of the APS division of fluid dynamics, pp 107-108, November 2012

Book contribution

[1] Jonathan Ferracci, Takuji Ishikawa, Hironori Ueno, Keiko Numayama, Yohsuke Imai, Takami Yamaguchi, Entrapment of fresh ciliates at the interface fluid-air, Nano-biomedical engineering 2012, pp 70-72, March 2012